Universidade de Aveiro Departamento de Ciências Médicas
2020

Mariana Brandão Moreira

Estudo do papel da Rabconnectina-3a nos corpos sinápticos das células ciliadas auditivas

Study of the role of Rabconnectin-3a at the auditory hair cell ribbon synapse

Universidade de Aveiro Departamento de Ciências Médicas
2020

Mariana Brandão Moreira

Estudo do papel da Rabconnectina-3a nos corpos sinápticos das células ciliadas auditivas

Study of the role of Rabconnectin-3a at the auditory hair cell ribbon synapse

Tese apresentada à Universidade de Aveiro para cumprimento dos requisitos necessários à obtenção do grau de Mestre em Biomedicina Molecular, realizada sob a orientação científica do Doutor Nuno Raimundo, Professor auxiliar convidado do Departamento de Ciências Médicas da Universidade de Aveiro e co-orientação científica da Doutora Ira Milosevic Professora auxiliar convidada do Departamento de Ciências Médicas da Universidade de Aveiro.

This work was supported by Schram-Stiftung T287/25457 and Deutsche Forschungsgemeinschaft (Emmy Noether Young Investigator Award MI-1702/1) to Ira Milosevic

This work was supported by an Erasmus+ grant provided in the context of the mobility Erasmus+ project.

Este trabalho é dedicado às pessoas que amo.

o júri

Presidente	Dr. Ana Gabriela da Silva Cavaleiro Henriques Professora auxiliar Universidade de Aveiro
Arguente	Professora Doutora Tina Pangrsic Vilfan Researcher Group Leader, University Medical Center Goettingen
Orientador	Dr. Nuno Filipe Viegas das Neves Raimundo Professor auxiliar convidado do Departamento de Ciências Médicas da Universidade de Aveiro

agradecimentos

I would like to thank my supervisor, Dr. Nuno Raimundo and Dr. Ira Milosevic for giving me this great opportunity to develop my Master Thesis abroad. I would also like to thank all the members from Raimundo and Milosevic labs, Dr. Mónica Costa, Dr. Renata Couto, Dr. Sindhuja Gowrisankaran, Katarzyna Wieciorek, Dr. King Faisal Yambire, UdhayaBhaskar SathyaNarayana, Dr. Johanna Castillo, Jin Jialin and lab technician Dirk Schwitters for all the help, advices and support. I would like to give a special thanks to Mónica Costa for the friendship and helpful guidance.

Queria também agradecer à minha família por serem a minha força.

palavras-chave

Rabconnectin-3a; Célula ciliada interna; Corpos sinápticos; V-ATPase; Otoferlin

resumo

As células ciliadas internas são as células sensitivas do órgão auditivo. A capacidade que demonstram para prolongar a atividade sináptica pode ser atribuída à presença de corpos sinápticos ancorados na zona ativa da sinapse das células ciliadas auditivas. Os corpos sinápticos são estruturas densas responsáveis pela ancoragem de vesículas sinápticas.

Rabconnectin-3a é uma subunidade do complexo rabconnectin-3. A rabconnectina-3a está presente nas vesículas sinápticas, mas também pode ser observada em outras estruturas neuronais. Este complexo é encontrado em abundância no cérebro, particularmente na sinapse, onde tem um papel importante na neurossecreção. A proteína Rabconnectin-3a é um conhecido regulador putativo da V-ATPase. Esta proteína é codificada pelo gene DMXL2. Estudos anteriores mostraram um papel importante desta proteína no desenvolvimento do cérebro. Sendo que as mutações no DMXL2 estão ligadas a deficiência auditiva e a distúrbios do desenvolvimento neurológico.

Assim, neste trabalho foi proposto estudar o papel da Rabconnectina-3a na sinapse da célula ciliada interna auditiva. Para atingir este objetivo, foi utilizado um modelo de murganho KO específico para a rabconnectin-3a nas células ciliadas internas, onde as partes apicais do órgão de Corti foram dissecadas e marcadas imunologicamente. Além disso, amostras de cóclea inteira foram preparadas e submetidas à técnica de Western Blotting (WB). Juntas, essas duas técnicas permitiram a quantificação dos níveis de proteínas, bem como a visualização da sua distribuição na sinapse da célula ciliada interna. Foi observada uma diminuição significativa nas subunidades da V-ATPase e na expressão da proteína otoferlin nos murganhos KO em comparação com os controlos Wild Type (WT), sugerindo uma diminuição no processo de reciclagem da vesícula sináptica.

Além disso, o número de corpos sinápticos observado nos murganhos KO foi maior comparativamente com o WT. O que pode ser devido a um comprometimento do desenvolvimento da sinapse. Por outro lado, os níveis das proteínas rabconnectin-3β e vGlut3 estão aumentados no modelo do murganho KO. De uma forma geral, os resultados obtidos neste trabalho forneceram novas informações sobre o papel da rabconnectina-3a na sinapse das células ciliadas internas de mamíferos.

keywords Rabconnectin-3a; IHC; Ribbon synapses; V-ATPase; Otoferlin

abstract

Inner hair cells (IHCs) are the sound sensing cells of the auditory organ. The synaptic activity capabilities that these cells have can be attributed to the presence of ribbons anchored in the active zone of the IHC synapse. The ribbons are an electron dense structures responsible for the tethering of synaptic vesicles. Synaptic vesicles are composed of lipids and many proteins, one of which is Rabconnectin-3a, a subunit of the Rabconnectin-3 complex. This complex is found abundantly in the brain, particularly at the synapses where it is important for neurotransmission. Rabconnectin-3a protein is a putative V-ATPase regulator with an important role in brain development. This protein is encoded by the DMXL2 gene. Mutations in the DMXL2 gene are linked to hearing impairment and neurodevelopmental disorders.

In this work it was proposed to study the role of Rabconnectin-3a in IHC ribbon synapse. To achieve this goal a Rabconnectin-3a knock-out (KO) mouse model in IHCs was used, where apical turns of the organ of Corti were dissected, immunolabelled and imaged. Also, the protein samples were prepared from the whole cochlea and subjected to Western blotting (WB) technique. Together, these two techniques have enabled the quantification of protein levels, as well as their distribution in the ribbon synapse.

A significant decrease in the expression of V-ATPase subunits needed for synaptic vesicle acidification and refilling, and otoferlin protein needed for calcium sensing were observed in the Rabconnectin-3a IHC KO mice in comparison with the Wild-Type (WT) controls, suggesting an impairment in IHC transmission. Also, the number of ribbons was higher in the Rabconnectin-3a KO IHC in comparison with the WT. This could be due to a developmental impairment. On the other hand, both Rabconnectin-3β (other component of Rabconnectin-3 complex) and vesicular glutamate transporter 3 (vGlut3) protein levels are increased in the Rabconnectin-3a KO mouse. Overall, the results obtained in this work provided new insights on the role of Rabconnectin-3a at the mammalian IHC ribbon synapse.

Table of contents

Chapter III. Results **Pages**

List of Abbreviations

IHC	Inner hair cell
OHC	Outer hair cell
rER	Rough endoplasmic reticulum
WT	Wild type
KO	Knockout
EAAT	Excitatory amino acid transporter
V-ATPase	Vacuolar-type ATPase
PBS	Phosphate Buffered Saline
EDTA	Ethylenediamine tetraacetic acid
PMSF	Phenylmethylsulfonyl fluoride
SDS	Sodium Dodecyl Sulfate
PCR	Polymerase Chain Reaction
DMSO	Dimethyl sulfoxide
ROI	Region of interest
vGlut3	Vesicular glutamate transporter 3
AAV1	Adeno-associated virus type 1
ER	Endoplasmic reticulum
RAVE	Regulator of the H^+-ATPase of vacuolar and Endosomal Membrane
NC	Neural Crest
EEA1	Early Endosome Antigen 1
CNVs	Copy number variations
ASD	Autism spectrum disorders
ADHD	Attention deficit hyperactivity disorder
PEPNS	Peripheral sensorimotor polyneuropathy-polyendocrine syndrome
GnRH	Gonadotropin-releasing hormone
EEG	Electroencephalography
SGCs	Spiral ganglion cells

List of Figures **Pages**

List of Tables

List of Materials

Reagent/ Material	Catalog Number	Company
Phosphate Buffered Saline	P4417-100TAB	Sigma Life Science
Tris-HCl	9090	Roth
IGEPAL	18896	Sigma Aldrich
Na-deoxycholate	30970	Sigma Aldrich
NaCl	P029.3	Roth
EDTA	8040.3	Roth
PMSF	6367,2	Roth
NaF	S7920	Sigma Aldrich
PhosSTOP phosphatase inhibitors	4906845001	Roche
Complete proteases inhibitors	87786	ThermoFisher
Homogenizer	431-0100	VWR Pellet Mixer
BCA protein determination assay	23227	ThermoFisher
Glycerin	3783.1	Roth
SDS	2326.2	Roth
β-mercaptoethanol	A1108.0250	Applichem
Brome phenol blue	A512.1	Roth
Gradient gel	456-1084	Bio Rad
PageRuler Plus Prestained Protein Ladder	#26619	Thermo Fisher
Tris base	5429.2	Roth
Glycine	3908.3	Roth
Nitrocellulose Membranes	1620115	Bio Rad
Methanol	8388,3	Roth
Milk powder	T145.4	Roth
Tween-20	9127.1	Roth
Proteinase K	7528,1	Roth
EtOH absolute	2246,1	Chemsolute
Promega Go Taq ® G2 Flexi DNA	M7806	Promega
DMSO	A994.1	Roth
Betaine	B0300	Sigma Aldrich
Agarose	840004	Biozym
Ethidium Bromide	E406-15ML	VWR
100bp DNA ladder	N3231S	Biolabs
Acetic Acid	7332.3	Roth
Formaldehyde	F8775	Sigma Aldrich
Goat Serum	1395813A	Invitrogen
Triton X-100	3051.3	Roth
Sodium monohydrogen phosphate	4984.1	Roth
Sodium dihydrogen phosphate	T879.2	Roth
DAPI	6335,1	Roth

Glass microscope slides	631-1553	VWR
Mowiol	A9011	Applichem
ANTIBODIES	**Catalog Number**	**Company**
Anti-DMXL2 antibody produced in rabbit	HPA039375	Sigma Aldricht
Mouse monoclonal Otoferlin antibody	Ab53233	Abcam
WDR7 antibody rabbit polyclonal	24431-1-AP	Protein Tech
Rabbit polyclonal Anti-ATP6V1A antibody	NBP1-33021	Novus Biologicals
Polyclonal rabbit purified antibody VGlut3	135 203	Synaptic Systems
Purified mouse Anti-CtBP2 antibody	612044	Transduction Laboratories
Polyclonal rabbit Anti-Homer	160 002	Synaptic Systems
Polyclonal rabbit Proton ATPase 116 KDa subunit	109003	Synaptic Systems
Polyclonal rabbit Anti-Rab 3a antibody	107 102	Synaptic Systems
Otoferlin	Custom-produced	Custom-produced
Anti-GAPDH produced in rabbit	G9545	Sigma
GAR800	926-32210	LI-COR
GAR680	926-68021	LI-COR
GAM680	926-68020	LI-COR
GAR488	A-11034	Invitrogen
GAM568	A-11031	Invitrogen
PRIMERS	**Sequence**	
VGLUT3-1 Oligo 13944	CCCGTGGGCTGGAGTTGAG	
VGLUT3-2 Oligo 13945	GCGCAGCAGGGTGTTGTAGG	
Cre^{+} 2 for	CCCCAGCAACTCCTCACTCA	
VGLUT3-2 rev	CAGCGAGTCTCCCACGGC	
Dmxl2-5Arm	ATCTGTGCCACAGACCTAGGAAGC	
Dmxl2-3Arm	GGAGAGCGGACACTAGTCCCTTGG	
Dmxl2-LAR3	CAACGGGTTCTTCGTTGTCC	

Chapter I. INTRODUCTION

1. Overview of the auditory system in mammals

The auditory system is divided in three main structures: the outer ear, the middle ear and the inner ear. The outer ear includes the auricle (also known as pina) and the tympanic membrane. The tympanic cavity (filled with air), the three ossicles and their attaching ligaments make the middle ear. Finally, the inner ear is inserted in the temporal bone and consists of the vestibular and auditory organs (**Fig.1A**) [1]. While the outer and middle ear are responsible for the transmission of sound as a mechanical wave, it is in the inner ear where it is transduced into action potentials that ultimately translate into our perception of sound [2].

In the inner ear, the auditory organ is also designated as cochlea. This spiral-shaped cavity outlined by the temporal bone has three chambers: the vestibular duct (scala vestibuli), the cochlear duct and the tympanic duct (scala tympani) (**Fig.1B**). Both the vestibular duct and the tympanic duct are filled with perilymph; this fluid has a comparable ionic composition to that of the extracellular fluid of the cells (low concentrations of K^+). However, the cochlear duct is filled with endolymph, which has a comparable ionic composition to that of intracellular fluid (high concentrations of K^+) [2]. The two outer chambers, vestibular duct and tympanic duct meet in the helicotrema, located in the cochlear apex. This interconnected two chambers surround and involve the cochlear duct [2].

In the cochlear duct, more precisely on top of the basilar membrane it is present the organ of Corti. This organ is composed of one line of inner hair cells (IHC) and three lines of outer hair cells (OHC) accompanied by supporting cells (e.g., Hensen's cells, Deiters' cells). The organ of Corti is responsible for the mechanoelectrical transduction of the sound stimulus (**Fig.1C**) [2]. One of the main features of the hair cells present in this organ is the hair bundle or hair cell bundle. These apical microvilli allows high sensitivity to sense pressure waves or movement in the fluid involving the structure [3]. The microvilli, also known as stereocilia of these hair cells sits on the cuticular plate (in the apical part of the cell) and extends towards the tectorial membrane, with the microvilli of the outer hair cells being directly linked to it. However, the inner hair cells microvilli aren't in direct contact with the tectorial membrane [1].

IHC are responsible for the majority of the cochlear electrical signals output release. This is due to 95% of the auditory afferent neurons' synapses with IHC, whereas the other 5% of afferent fibres synapses with outer hair cells [2]. In terms of

function one can say that the IHC are the sensory receptors and the outer hair cells' main function is to promote the amplification of the signal, playing a modulatory role [1].

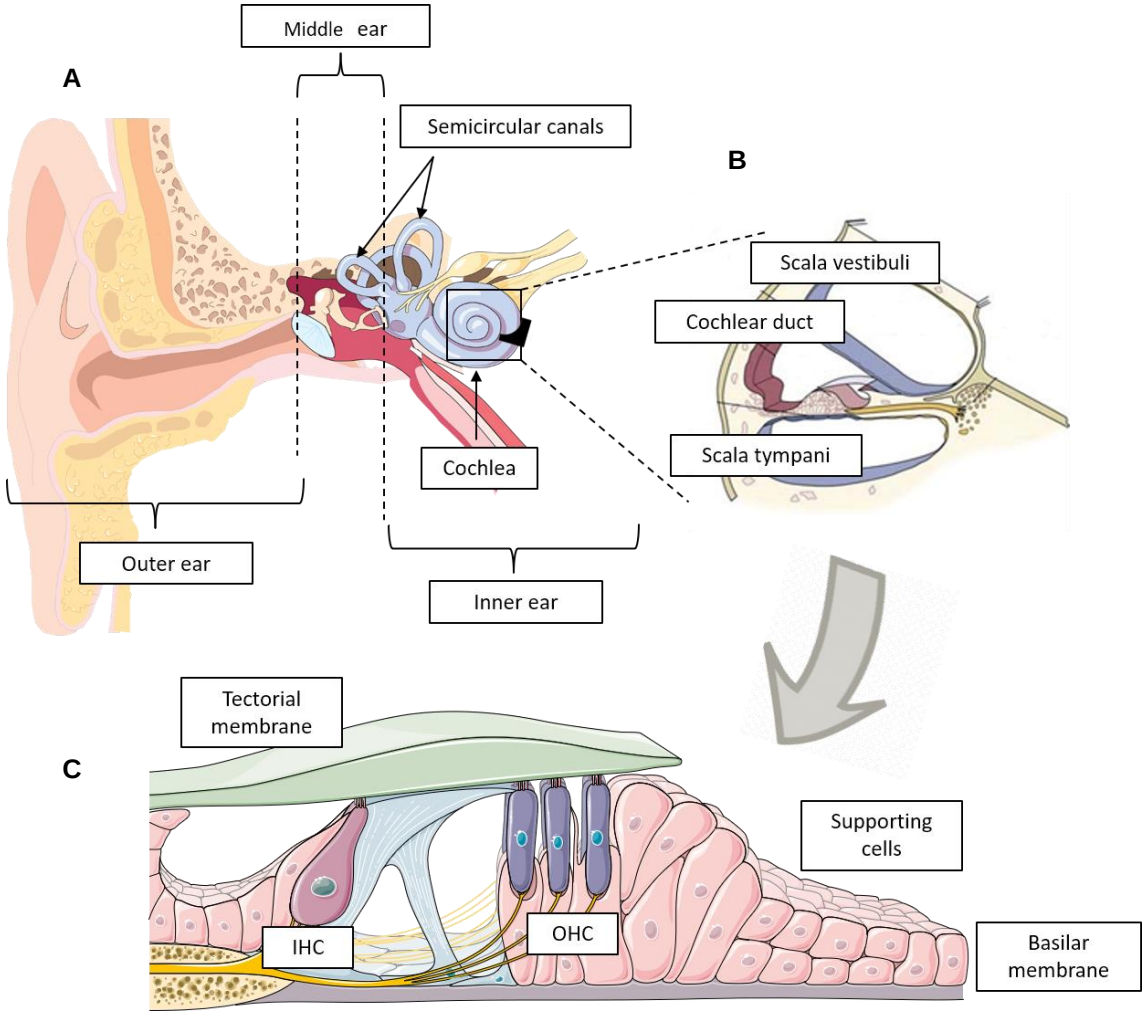

Figure 1. Structure of the mammalian inner ear | (A) Overview of the three main structures of the mammalian ear (outer, middle and inner ear). **(B)** Cross-section through the cochlea, showing the three fluid-filled cavities (scala vestibuli, cochlear duct and scala tympani). **(C)** Organ of Corti in detail. It is constituted by one row of IHC and three rows of OHC surrounded by a variety of supporting cells. All these cells are settled in the basilar membrane. Images modified from Cummings Otolaryngology: Head & Neck Surgery, Anatomy of the Auditory System Cochlear Anatomy Osteology [4].

1.1. Mechanoelectrical transduction of the sound stimulus

In order to detect and understand the sounds that surround us we need to translate the mechanical waves into nerve impulses that then can be perceived by our brain as sound.

The pina focus the sound waves through the ear canal towards the tympanic membrane. When these pressure waves arrive at the tympanic membrane, they make it vibrate. These vibrations are then transmitted to the three bones of the middle ear, malleus, incus and stapes, respectively. Then the stapes transmits these vibrations into the outermost structure of the inner ear, the oval window. This flexible membrane makes the separation between the air-filled cavity of the middle ear and fluid-filled cavity of the inner ear. Thus, these vibrations generate pressure waves in the fluid (perilymph) and lead to the vibration of the basilar membrane and consequently the deflection of the hair bundles of the hair cells against the tectorial membrane situated just above [2].

In order to achieve the same response from all hair cells, microvilli present in the hair bundle must all be aligned and oriented in the same direction [2]. Bearing this in mind, microvilli deflection in one direction increases the probability of the opening of the mechanically gated ion channels present on the top of the hair bundle and enables the influx of ions into the cell causing depolarization. This depolarization promotes the opening of the voltage gated calcium channels present in the soma of the cell and lead to the release of neurotransmitters (**Fig.2**). However, the displacement of these hair bundles in the opposite direction decreases the probability of the opening of the mechanically gated ion channels, therefore resulting in the hyperpolarization of the cell [1].

IHC are the ultimate translators of sound waves into action potentials. To understand in detail how this process unfolds, we need to know the IHC features that make them so efficient in their role.

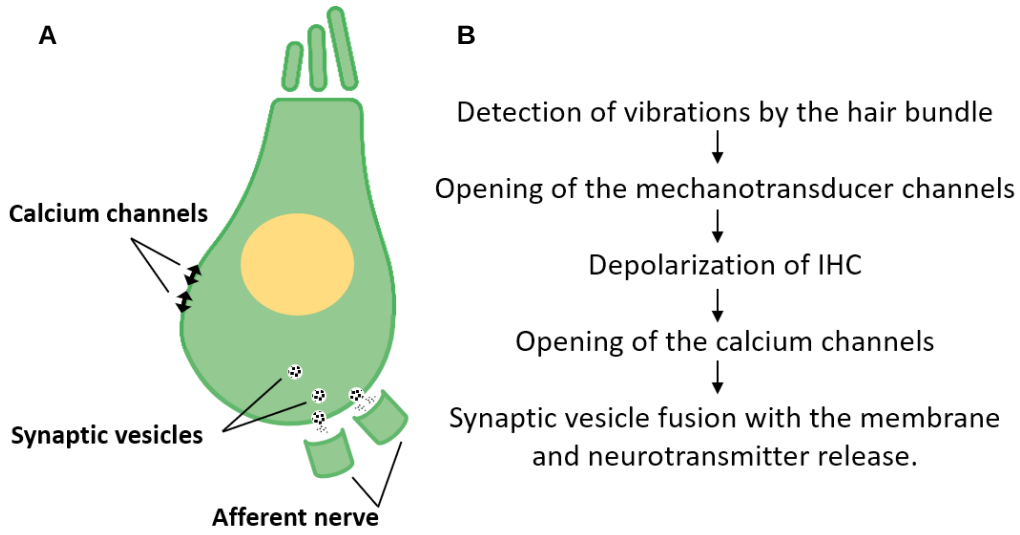

Figure 2. Overview of the mechanoelectrical transduction at the IHCs | (A) IHC showing the hair bundle, responsible for the detection of vibrations. The calcium channels in the basolateral membrane is responsible for the triggering of synaptic vesicle fusion with the membrane and exocytosis. Then the neurotransmitters released in the synaptic cleft bind to their respective receptor present in the post synaptic zone in the afferent nerve. **(B)** Illustrative outline of the main steps of synaptic transmission by the IHC. From the movement of the hair bundle to the neurotransmitter release in the basal region of the cell.

2. Inner hair cell (IHC) morphology

IHC are without any doubt the sound-sensing cells of the organ of Corti. Their sensory epithelium converts sound-induced vibrations into electrical signals that are then directed to the brain via post synaptic nerve. The contact established with the post synaptic nerve is located specifically in the infranuclear region and each cell can be innervated by up to 20 afferent nerve fibres [5].

Known by their “flask” form with a constriction in the apical or neck region, their cell body is oriented towards the core of the cochlear spiral (the modiolus) and the nucleus is in the apical part of the cell. Evidence of an enriched and continuous network of intracellular membranes across the infranuclear region has been described as “canaliculi”. These intracellular membrane systems seem to run from the part below the nucleus to the plasma membrane in the basal area near the synapses [6]. In addition Anwen Bullen et al. [7] reported that these same intracellular membrane systems appeared more extensively in the flattened side of the cell alongside with the mitochondria (in which the two form a

complex) and afferent terminals are concentrated (**Fig.3**). In previous studies microtubule tracks have been described as longitudinally oriented (between the apex of the cell and the basal part), similarly to the orientation presented by the membranes [7].

Interestingly, small vesicles tethered to rough endoplasmic reticulum (rER) were observed by high-resolution electron tomography. Despite rER being often associated with vesicle trafficking between the Golgi complex and the rER itself for synthesis products exchange, Golgi complex was absent in the infranuclear region. In addition, vesicles spotted in the location were not fusing with the rER membrane, instead they were tethered to it by filamentous linkages. These observed vesicles were suggested to be neurotransmitter vesicles based only in their small size. Vesicular glutamate transporter 3 (vGlut3)-immunolabelled IHC showed the presence of this glutamate transporter throughout the cytoplasm of the cell and not just concentrated at the synapse, suggesting that the membrane network works as a secondary store of synaptic vesicles for release during sustained synaptic transmission. Therefore, the regulation functions of the rER allied to the mitochondria role might create a multifunctional complex with the ability to orchestrate the synaptic provision and neurotransmitter release [7].

However, there are other important features that make IHC an efficient tool of signalling. One of them is that they are endowed with a strong polarization in both short and long axes. Showed by the compartmentalization in the apicobasal axel, where we have in the apical part of the cell the mechanoelectrical channels and on the basal part of the cell the voltage gated channels which transduces in the efficient generation of graded receptor potentials [8].

Therefore, one can suggest that the mature IHC of the mouse can be subdivided into two distinguished regions:

1- A supranuclear region enriched with cells machinery in the form of Golgi bodies and endoplasmic reticulum (ER) responsible for protein synthesis;
2- An infranuclear region where a network of ER, mitochondria, ribbon synapses and vesicles are present.

In fact, the ability to drive rapid, precise and sustained synaptic release by the IHC results in part by the presence of synaptic ribbons. They are a specialized structure that are anchored in the active zone of the synapse and are encircle by synaptic vesicles [7]. Therefore, in the next topic the active zone as well as the ribbon synapse will be addressed with more detail.

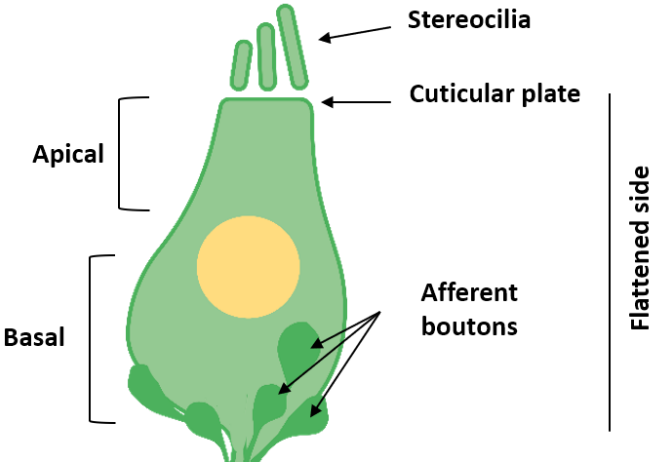

Figure 3. IHC structure | The IHC is "flask" shaped and presents a constriction in the apical region. The stereocilia of the hair bundle rest in top of the cuticular plate and afferent terminals are more concentrated in the flattened side of the cell.

3. IHC ribbon synapse

Synapses are constituted by a presynaptic site where the numerous synaptic vesicles wait for the stimulus to trigger their fusion with the IHC membrane at the active zone, a synaptic clef where the neurotransmitters are released to, and a postsynaptic site where the neurotransmitters bind with the respective receptors. A big variety of presynaptic proteins oversee neurotransmitter release at the active zone. They can be separated into three main sections classically referred to as:

1. The cytomatrix at the active zone (CAZ);
2. Presynaptic electron dense projections that are clustering synaptic vesicles and organize release;
3. Synaptic vesicles [9].

To encode acoustic stimulus with high precision the active zone of the ribbon has a tough assignment, the tireless and rapid release of synaptic vesicles and followed by recycling at individual synapses. Indeed, sustained exocytosis is an essential requirement to regulate the release of neurotransmitters can follow acoustic stimuli with a periodicity of 1 ms or less [10], [11], [12], [13], [14], [15]. Both rapid on and off kinetics are required for the quick clearance of previously exocytosed substances as well as priming of new vesicles that are ready for the release. In other words it is required an efficient system to allow the extensive synaptic vesicle cycling [8].

The neurotransmitter release is mainly controlled by the Cav1.3 Ca^{2+} channels [16], [17], [18] and evidence showed by various techniques indicates that these channels are clustered at the ribbon active zone of the hair cell [19], [20], [21], [22], [23], [24], [18].

The ribbon is an electron dense structure present in the active zone of the presynaptic cell and it's responsible for the tethering of synaptic vesicles [25]. These structures exist also in the outer hair cells [26]. The protein RIBEYE is the main component of the ribbon synapses of mouse cochlear hair cells [27].This protein is composed by two domains and both of them play a role in the ribbon synapse. The A domain is responsible for the assembly of the ribbon and the B domain (very similar to the transcription repressor CtBP2) is believed to be involved in the tethering of synaptic vesicles to the ribbon [28], [29].

Another protein found in the active zone is bassoon. This scaffold protein is believed to play a role in the anchoring of the ribbon at the active zone site [30], [31], [27]. Additionally, partial deletion of the gene that encodes this protein showed a decrease in the amplitude of readily releasable pool of synaptic vesicles [27] and a slight reduction of the calcium currents (which point to a reduced insertion of calcium channels in the active zone). Therefore, there is possibly an important contribution of bassoon for not only the anchoring of ribbon but also in the organization of the active zone [25].

In conventional synapses both bassoon and its homolog piccolo are expressed, however in IHC synapses piccolo is substituted by is short isoform piccolino (main feature is the lack of the large C-terminal part) [32], [33]. Studies carried out in piccolino RNAi-based knockdown showed an impairment in the formation of the plate-like structure of the ribbon and thus suggesting an important role of this protein in the structural maturation of the ribbon [33].

Altogether, these proteins play an important role in ribbon anchoring to the active zone and are their main structural components [8].

3.1. Ribbon function

In fact, the capability that the IHC shows to prolong synaptic activity for long periods of time can be attributed to the presence of ribbons anchored in the active zone of the IHC synapse.

Many hypotheses have been suggested to clarify the ribbon function:

1. Enable a large readily releasable pool of vesicles [27], [34].
2. Benefit vesicle replenishment at the active zone [35], [36], [37], [38], [39].
3. Promote multivesicular release [40], [41].
4. Allows high calcium concentrations and thus makes up has a diffusion barrier [42].

Vesicles ribbon-associated are situated around the ribbon and connected to it through filamentous proteins tethers (**Fig.4**). The vesicles located in the basal part of the ribbon are also connected with the pre-synaptic membrane (membrane-proximal vesicles). Further away from the population of vesicles associated with ribbon, the presence of other vesicles close to or even connected (tethered) to the membrane are also observed. It is suggested that these membrane-proximal vesicles make the readily releasable pool. The similarity between the functional size of the readily releasable pool and the estimated number of membrane-proximal vesicles [43], [44], [34], accompanied by the observation that these same vesicles are highly used up after stimulation [45], [44], all support this suggestion. To add to the evidence found, fusion capability can be correlated to the ability of the vesicles to tether to the active zone [46], [34], [47]. The ribbon is also been associated with vesicle biogenesis [48].

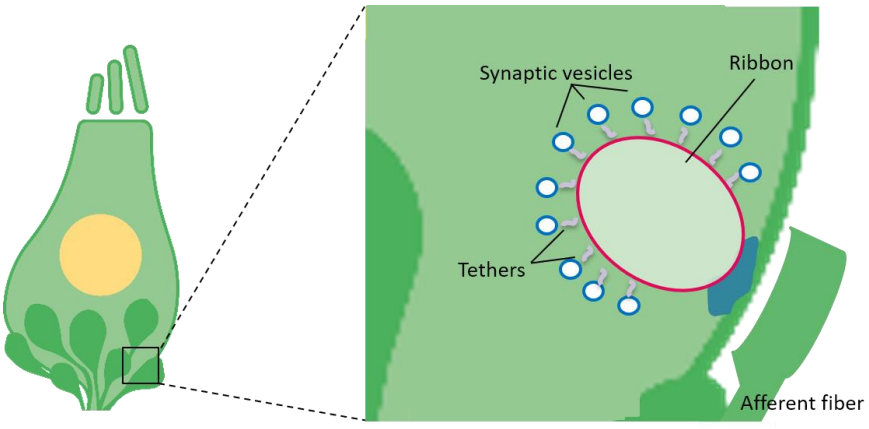

Figure 4. Ribbon-associated vesicles at the IHC ribbon synapse | The ribbon is a specialized synaptic dense structure responsible for the tethering of synaptic vesicles. They are anchored very close to the cell membrane at the active zone of the synapse. The synaptic ribbon is attached to the active zone membrane by a presynaptic density (evidenced in blue).

4. Maturation of IHC ribbon synapses in the apical mouse cochlea

Ribbon synapses of IHCs go through a variety of functional and structural changes that ultimately result in an efficient and functional ribbon synapse. These set of processes are known by ribbon synapse maturation. The hearing onset of mice occurs on postnatal day P(12) [49]. Before this timepoint, the active zone of the mice IHC is very distinct, showing different morphology. For example, calcium channels that are located extrasynaptically are gradually removed from the nonsynaptic basolateral plasma membrane jointly with the respective postsynaptic glutamate receptors and create dense clusters at mature presynaptic active zones [34], [50]. Another important change that occurs in the first postnatal week of development is the substitution of synaptotagmins by otoferlin (a large Ca^{2+} binding multi-C_2 domain protein) making this protein the main calcium sensor of the IHC. Recent findings indicate that synaptic contact formation precedes ribbon attachment at the active zone of the membrane [51]. Therefore, the establishment of synaptic connectivity is one of the first steps in the developmental and maturation process in IHC. Another important step is the fusion of floating ribbon precursors to membrane attached ribbons or even the fusion of membrane-anchored ribbons. The precursor ribbons are suggested to be formed in a distant site from the active zone because floating precursors were found along with tethered synaptic vesicles in the cytosol of the cell. The fusion process enables ribbon number reduction while modulating ribbon size and assuring the formation of functional ribbons. Interestingly, a comparison between ribbon volume at P9 and P34 IHCs showed similar ribbon volumes implying that RIBEYE levels in the presynaptic zone remain approximately constant throughout synapse maturation, independently of ribbon number. In the presynaptic zone the confinement of Ca^{2+} channel clusters transformation of Ca^{2+} micro to nano-domain like regulation of exocytosis as well as synaptic vesicle maturation and establishment of glutamate pathways are all structurally crucial steps for ribbon synapse formation. Therefore, when adult synaptic configuration is established it's possible to spot an increase in synaptic vesicles number and decrease of their diameter. Nevertheless, few multiribbon synapses remain into adulthood.

In summary, following chronological order, the main changes can be listed as follow:

1. The establishment of afferent contacts between IHC and SGNs (spiral ganglion neurons) and then ribbon attachment at the presynaptic membrane;

2. Both ribbon size and synaptic vesicle population increase until the hearing onset whereas the diameter of synaptic vesicles decreases throughout maturation process;

3. Ribbon precursors at the presynaptic site, are fused together in order to generate functional and mature single ribbons;

4. Ribbon precursors are evidenced as making use of active mode of transport to the active zone of the IHC (**Fig.5**) [51].

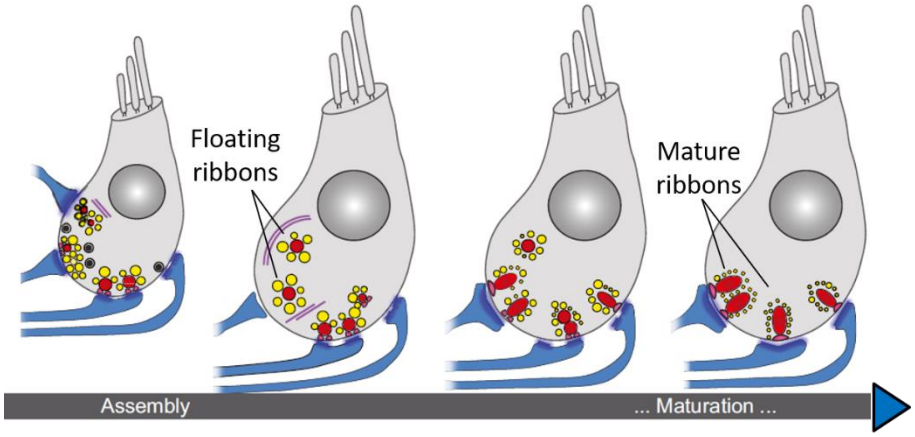

Figure 5. Ribbon maturation in IHC | Schematic diagram of ribbon maturation steps. Ribbons are represented in red the synaptic vesicles tethered to them are in yellow and microtubules are represented as purple lines. Floating ribbons are guided to the active zone of the IHC synapse, and then they fuse together with already membrane-attached ribbons leading to ribbon number reduction while regulating ribbon size. Adapted from [51].

5. Synaptic neurotransmission: synaptic vesicle neurotransmitter filling

Synaptic transmission is mediated by glutamate neurotransmitter release. The transport of the excitatory amino acid glutamate into the synaptic vesicle is orchestrated by a family of vesicular glutamate transporters, a set of three, vGlut1, vGlut2 and vGlut3 to be more precise [52], [53]. Therefore, vGlut3 is very important in the filling of the vesicles with neurotransmitters because it's responsible for the exchange of protons by the neurotransmitter glutamate [54], [55], [56], [57]. IHCs express vGlut3 and the absence of this protein in mice IHC results in deafness due to loss of glutamate release at the IHC afferent synapse [57]. Interestingly, studies have also showed that mutations in the human gene SLC17A8 (gene that encodes vGlut3), might underlie the high frequency hearing loss of autosomal dominant DFNA25 locus at 12q21-24 [56].

In a study conducted in vGlut3 KO mice, ribbons at the IHC synapse presented a thin and elongated form, similar with the one described in otoferlin KO mouse [58].

Another interesting finding was the fact that the vGlut3 KO mice partially rescued using adeno-associated virus type 1 (AAV1) transgene expression in only IHCs presented a higher number of synaptic vesicles tethered to the ribbon in comparison with the WT. In addition, vGlut3 expression levels quantification by RT-PCR showed increased levels in rescued animals in comparison with WT. Although, RT-PCR data may suggest an association between vGlut3 mRNA expression levels and vesicle number this does not prove that all of those vesicles are properly packaged. In fact the authors refer that continuous production of vGlut3 by the viral promoter may prevent the IHC from properly packaging the vesicles at a normal rate, leading to a higher number as well as a mixture of regular and irregular-appearing vesicles [59].

In fact, in order to facilitate the exchange of protons for neurotransmitter filling into the synaptic vesicles, the process of acidification must take place [60], [61], [62]. This acidification depends on the vacuolar-type ATPase (V-ATPase) and it is the main electrochemical driving force responsible for this process to happen. The V-ATPase complex has two main units, V_1 that corresponds to the cytosolic unit and V_o that corresponds to the membrane unit. These units are composed by many subunits and the membrane and cytosolic units, despite being essentially assembled can be disassembled [63], [64], [65]. V_1 peripheral domain is composed by eight different subunits (A-H) and is responsible for ATP hydrolysis while the V_o domain is responsible for proton translocation. V-ATPase make use of a rotatory mechanism in which ATP hydrolysis within the V_1 domain triggers the rotation of the rotatory complex constituted by subunits D, F, d and the proteolytic ring [66] . Thereby, the function of V-ATPase is essential insofar as it is responsible for the concentration of protons in the lumen of the vesicles [61], [62]. There are various mechanisms responsible for V-ATPase regulation. One of the earliest identified was the reversible disulfide bond formation between conserved cysteine residues within the catalytic site of V-ATPase [67]. Another important regulation mechanism described involves modulation of pump density, which is important in the regulation of proton transport across the membrane of epithelial cells. A third mechanism of V-ATPase regulation is related to reversible dissociation of the V_1 and V_o domains. Another mechanism gives account on changes in the coupling of proton transport and ATP hydrolysis. And finally, a mechanism of vacuolar acidification that involves changes in transporters other than V-ATPase [66].

V-ATPase activity can also be modulated by additional regulatory proteins and one of the example is the rabconnectin-3 complex. This will be a topic addressed here in detail (more information on Rabconnectin-3a is presented below).

6. Synaptic vesicle tethering and exocytosis

Notably, the synaptic ribbon in which synaptic vesicles are tethered is a characteristic feature of IHC synapses. Observing the IHC synapse, different morphological stages of synaptic vesicles close to membrane can be spotted. Heterogenous tethers regarding number and length are noticed in the active zone and are responsible for the connection of the vesicles to the active zone membrane both in conventional synapses and synaptosome preparations [68], [46], [69] ,[47] as well as in IHC ribbon synapses [34]. Furthermore, studies conducted in synaptosomes prepared from hippocampal tissue using cryo-electron tomography techniques, suggested that the vesicles entered in the readily releasable pool by the formation of short tethers. It was then revealed that tethering of the vesicles precedes the full contact of the vesicle with the membrane [69]. Another relevant fact is that the action of tetanus toxin causes inhibition of this short tether formation, in turn suggesting that SNARE proteins take part in this procedure [69].

Munc13 and CAPS, priming factors, seem to not operate in IHC ribbon synapses [70], contrarily to what happens in conventional central nervous system synapses, where Munc13-1 [71], [46], [47] and Rimα are involved in the process of vesicle tethering. Thus, a hypothesis was proposed in which the ribbon is endowed with the priming function [39].

In other systems SNARE proteins like syntaxin 1, SNAP25 and synaptobrevin 1 play a key role in exocytosis [72], [73]. These proteins are also present in the IHC synapses [74]. However, in IHC synapses the role of these proteins in exocytosis is not assured, because when performed genetic ablation of neuronal SNAREs or applied neurotoxins treatments no significant change was observed [75]. Furthermore, synaptotagmins 1-3 [76], [77], complexins [78], [79] and SNARE regulators seem to be missing in mature IHC. Indeed, the main proteins involved in the process of vesicle function differ significantly from the so called ‘conventional’ central nervous system synapses [8].

One protein that plays an important role in exocytosis at the IHC synapses is otoferlin [58], [80], [81], [44]. The lack or mutation of this multi-C_2 domain protein resulted in hearing impairment or even in deafness, both in humans [82], [83], [84] and rodents [58], [85], [86]. Otoferlin is mainly found at synaptic vesicles and in the active zone membrane [58]. Due to its high capability to bind calcium [58], [87], [88], [89], [44] it’s suggested that it can act as a calcium sensor [58], [89]. Thus, being necessary for the correct vesicle fusion and replenishment [58], [44], [90].

To better understand the cascade of events that result in neurotransmitter release, explanation step by step of these events will be addressed. Firstly, synaptic vesicles are guided to the fusion site of the presynaptic membrane via protein-protein interaction. The proteins responsible for this mechanism are SNARE proteins, proteins of the Rab family and Munc18 [91], [92]. Then the SNARE complex is formed by the interaction of syntaxin1 and SNAP25 (which are mainly observed anchored to the presynaptic membrane [93], with vesicle-associated membrane protein (VAMP/synaptobrevin). This complex is responsible for the approximation of the synaptic vesicle and plasma membrane at the fusion site [91], [94]. All these SNARE proteins are expressed in IHCs which may suggest an involvement of these proteins in neurotransmitter release in these cells [74]. Studies conducted in Otof $^{-/-}$ mice evidenced similar number of vesicles tethered to ribbons in both Wild Type (WT) and Knockout (KO) mice, which suggests that otoferlin absence does not impair synaptic vesicle biogenesis or docking. Therefore, otoferlin may play a role downstream of the docking step.

In central nervous system synapses, once the synaptic vesicle is docked to the presynaptic plasma membrane, the priming step takes place. This maturation step involves Munc13-1 protein as well as other factors [95] and it's crucial for Ca^{2+} triggered neurotransmitter release. Thus, increase of Ca^{2+} concentration, drives Syt I to bind up to five Ca^{2+} ions and enables fusion of the already primed vesicles with the plasma membrane in a SNARE-dependent way.

Exocytosis is essential for the transmission of the sound signal. Precise and reliable information must be encoded by the action potentials generated by the neurotransmitter release. Many hypotheses of how exocytosis occurs have been suggested, namely:

1. Several individual vesicles fusion occur in a synchronized way;
2. Homotypic vesicle-to-vesicle fusion before compound fusion (process in which vesicles fuse with already fused vesicles resulting in a wave of exocytosis, [96].
3. Ongoing homotypic vesicle-to-vesicle fusion and release occurs simultaneously [97], [40], [98].
4. Dynamic vesicular fusion pore controls univesicular release [99].

It is still not clear how this process takes place in IHC. When vesicle fusion, followed by release doesn't occur, it is necessary to have another mechanism that mobilizes the vesicle to the membrane. One of the first models addressing the neurotransmitter release in IHC proposed was the 'conveyor belt' model [35], [36], [37], [38]. Most recently, ribbon tethers are believed to play a role in the trafficking of the vesicles to the membrane

through a process called ‘crowd surfing’, where the tethers connect the vesicles and stop them from diffusing until they arrive to the active zone membrane [100]. The passive diffusion is maintained by a gradient established by the release of exocytic vesicles at the base of the ribbon [100]. The neurotransmitter release into the synaptic cleft activates the AMPA-like receptors located in the postsynaptic density (PSD) of afferent auditory fibres. In order to clear the synaptic cleft and avoid excitotoxicity due to high amounts of glutamate neurotransmitter, glutamate transporters (excitatory amino acid transporter, EAAT) pick up glutamate and enable its mobilization into supporting cells [101], [102], [103].

7. Rabconnectin-3a is a putative V-ATPase regulator

Rabconnectin-3 protein is comprised by two subunits, Rabconnectin-3a and Ranbconnectin-3β. Rabconnectin-3 is abundantly expressed in the rat brain. Immunofluorescence and immunoelectron microscopy of mouse hippocampus along with primary culture of rat hippocampal neurons have shown that this protein is associated with synaptic vesicles at the synapse. In fact, Rabconnectin-3a and Rabconnectin-3β were originally identified from purified synaptic vesicles fractions of rat hippocampus, suggesting a role of rabconnectin-3a in synaptic function [104], [105].

As this protein has no transmembrane segment and can be drawn from the vesicle with the use of a detergent, Rabconnectin-3 is considered a peripheral membrane protein of the synaptic vesicles [104]. Therefore, this complex concentrates mostly in synaptic vesicles at the synapse and it is very important in neurosecretion [104], [105], [106].

Rabconnectin-3a is encoded by the DMXL2 gene present in the 15q21.2, this subunit makes part of the rabconnectin-3 complex. It’s constituted by 16 WD repeat domains and consists of 3036 amino acids [107]. The molecular weight of this protein is approximately 340 KDa (**Fig.6**). Both Rabconnectin-3a and Rabconnectin-3β proteins belong to the WD40 family of proteins. These WD40 domains are responsible for the formation of a β-propeller structure that interacts with various proteins engaged in several cellular processes such as signal transduction, autophagy and apoptosis [108], [109].

Studies in Drosophila epithelial cells showed that in the absence of both Rabconnectin-3a and Ranconnectin-3β, Notch signalling is disrupted due to abnormal acidification of intracellular compartments. Along with these findings Rabconnectin-3a and Rabconnectin-3β were also suggested to play a role in endocytic trafficking, since mutations in both subunits caused accumulation of Notch and other membrane proteins in

late endosomal compartments [110]. In Sethi et al. study Rabconnectin-3 was shown to be a functional regulator of mammalian Notch signalling being required for proper Notch signalling [111].

Another study conducted in zebrafish deficient Rabconnectin-3a or Atp6Voa1 evidenced impairment in Neural Crest (NC) cells migration and misregulation of cadherins expression. It was also reported that Rabconnectin-3a loss of function initially downregulates several Wnt targets engaged in epithelial mesenchymal transition. Impairments in endocytosis were also observed, once the NC cells of Rabconnecin-3a or Voa1 deficient embryos showed an accumulation of Early Endosome Antigen 1 (EEA1) positive acidified endosomes and a decrease of late endosomes/lysosomes, which translate in an essential role of Rabconnectin-3a in endosome formation and maturation. However, endosome acidification was not found compromised implying that Rabconnectin-3a is not required for their acidification. Therefore, Rabconnectin-3a plays an important role in the regulation of vesicle endocytosis and Wnt signalling during NC migration [106].

In the zebrafish inner hair cells, rabconnectin-3a was found in the basal region overlapping the area where synaptic vesicles are enriched [112]. Studies conducted in mice showed also the enrichment of rabconnectin-3a on the basal region of the hair cells and on the end of the neurofilaments of spiral ganglion neurons, implying a role of this protein on both presynaptic and postsynaptic sites [113]. Several studies support a role of rabconnectin-3 in the modulation of V-ATPase activity, namely:

1. Recent studies conducted in Drosophila ovarian tissue and mammalian cell lines evidenced that rabconnectin-3 complex was required for acidification of intracellular compartments [114], [111].
2. In coimmunoprecipitation experiments one of the subunits of rabconnectin-3 complex, Rabconnectin-3β was found to interact with subunits E and H of V1 ATPase in insects [114].
3. Studies conducted in zebrafish demonstrated that Rabconnectin-3a mutant hair cells failed to properly acidify synaptic vesicles and lower levels of V_1a protein expression was found at basal region resulting in the impairment of synaptic transmission in comparison with WT [112].
4. In yeast models V_1/V_o assembly/disassembly is sustained by RAVE (Regulator of the H^+-ATPase of vacuolar and Endosomal Membrane) complex [63], [115]. This heterotrimeric protein complex is constituted by Rav1, Rav2 and Skp1 proteins. As Rav1 is absent in vertebrates and mammalian orthologue protein is

Rabconnectin-3a, supporting the hypothesis to have the same function in higher eukaryotes [104].

All these evidences suggest that Rabconnectin-3a plays an important role in the regulation of V-ATPase activity on synaptic vesicles and consequently in successful synaptic transmission [112]. Apart from the involvement in synaptic vesicle acidification, the impairment in Rabconnectin-3a could impact synaptic transmission by other pathways, like vesicle fusion or trafficking. Interestingly, both Rabconnectin-3a and Rabconnectin-3β were shown to form a complex with Cav2.1 and Cav2.2 channels in mouse brain. Thus, both subunits have a direct impact in current density, suggesting a possible regulation role in brain function by presynaptic calcium influx [116].

Originally the rabconnectin-3 complex was believed to act just like a scaffold in which Rab3 GEP and GAP to regulate Rab3 activity [104], [105]. Rab3 activity specifically influences calcium dependent exocytosis, Rab3-dependent cargo trafficking to the synapse and possibly nucleation of the synapse [117], [118], [119].

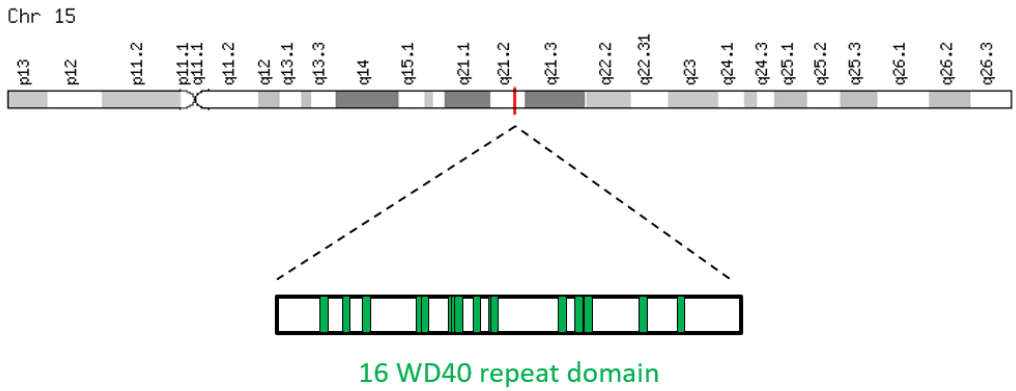

Figure 6. DMXL2 gene localization in Chr 15 | Representation of the 16 WD40 repeat domains. WD40 domains are believed to form a circularised beta-propeller structure. These WD40-repeat proteins are involved in functions such as signal transduction, autophagy and apoptosis [109].

8. Rabconnectin-3a links to diseases

Several pathologies have been associated with DMXL2 mutations. In fact, DMXL2 KO mice are embryonic lethal [120], [121] and heterozygous DMXL2 ($DMXL2^{+/-}$) mice revealed an important role of this gene in brain development by the presence of macrocephaly and corpus callosum dysphasia in mice carrying that mutation [122].

Additionally, heterozygous copy number variations (CNVs) jointly with loss-of-function single nucleotide variations involving DMXL2 are spotted in patients with various neurodevelopmental disorders, such as autism spectrum disorders (ASD), intellectual disability or even attention deficit hyperactivity disorder (ADHD). All these evidences lead to the hypothesis that DMXL2 haploinsufficiency might be linked to these same diseases acting like a predisposing factor [123].

Another study regarding DMXL2 haploinsufficiency reports that a homozygous in-frame deletion of 15 nucleotides in DMXL2 gene is present in three brothers in which is observed growth retardation, moderate intellectual disability accompanied by progressive hearing loss and peripheral sensorimotor polyneuropathy-polyendocrine syndrome (PEPNS) [120], [124]. The conditional heterozygous deletion of DMXL2 from mouse neurons carried out in the study presented a lower number of gonadotropin-releasing hormone (GnRH) neurons in the hypothalamus of adult mice in which Rabconnectin-3a is expressed in exocytosis vesicles present in the axonal extremities. This decrease results in the delay of puberty and in low fertility. Interestingly, also in the same study, DMXL2 knockdown in an insulin-secreting cell line evidenced impaired glucose metabolism. Being that the decrease of Rabconnectin-3a led to an increase in spontaneous insulin release accompanied by the disruption of glucose-induced insulin regulation. This suggest that Rabconnectin-3a has a modulatory role in insulin secretion in vivo. Thus, all these findings indicate a modulatory role of rabconnectin-3a in neuronal and endocrine homeostatic mechanism [120]. In other study also regarding Rabconnectin-3a and GnRH neurons, it was shown that Rabconnectin-3a has a role in the maturation of GnRH and establishes the capacity of GnRH activation by kissepeptin and estradiol [125]. In another recent study by Chen et al, DMXL2 mutations were linked to hearing impairment. In this study a large Chinese Han family was subjected to a genome sequencing where a heterozygous missense variant in DMXL2 was associated with dominant, nonsyndromic hearing loss [113]. Interestingly the phenotype portraited is very similar to the one presented by the vGlut3 KO mice in which the mutation translates into a hearing impairment [59].

In another study conducted in humans, it was demonstrated that biallelic loss-of-function DMXL2 mutations in six children causes a severe phenotype linked to Ohtara

syndrome, with profound neurological impairment, sensorineural deafness, moderate peripheral polyneuropathy, persisting burst suppression electroencephalography (EEG) pattern and dysmorphic features. After functional studies performed in the patient's fibroblasts, it was reported that the absence of Rabconnectin-3a resulted in impairment of lysosomal function alongside with the autophagy impairment [126].

8.1. Rabconnectin-3a and hearing impairment

Until now many genetic studies have been carried out in mice, zebrafish and humans in order to discover new insights of the hearing process [127], [128], [129].

A recent study conducted in a large Chinese Han family identified a heterozygous missense variant of DMXL2 gene that is linked to dominant, non-syndromic hearing loss in humans [113]. DMXL2 gene has already been identified in a zebrafish balance and hearing mutant, representing an example of hereditary deafness gene in zebrafish. In that same study, the Rabconnectin-3a mutant zebrafish had relatively mild to moderate auditory and vestibular effects in comparison with other zebrafish mutants, such as vGlut3 and Ca1.3a. Regarding the synaptic morphology no significant changes were observed, being that both pre and post synaptic zones appeared to be normal. In order to determine if these Rabconnectin-3a mutant zebrafish had a synaptic vesicle acidification impairment, lysotracker was used in the zebrafish IHCs. A massive reduction of this membrane-permeable vital dye was evidenced in the mutant zebrafish translating into synaptic vesicle acidification impairment. Another important finding was the fact that Rabconnectin-3a is essential for trafficking and assembly of V_1 subunit of the complex. Therefore, Rabconnectin-3a plays an important role in synaptic vesicle acidification and V-ATPase localization in zebrafish animal model [130].

9. Aim of the study

Currently there is no mammalian model to study DMXL2-related human hearing loss. This study builds on the novel model generated in Ira Milosevic's laboratory in Göttingen, Germany (described below) and it explores the changes in Rabconnectin-3a IHC KO mice comparatively to WT. As it has been stated before, Rabconnectin-3a is essential for functional synaptic transmission, so the complete lack of Rabconnectin-3a in mouse is lethal. Using tissue-specific Rabconnectin-3a KO mice (specific for organ of Corti), the key goal is to understand the specific role of Rabconnectin-3a in the IHC morphology. To this end, expression levels and distribution of key proteins involved in IHC synaptic vesicle recycling were examined in KO mice in comparison to WT. In the first aim, apical parts of the organs of Corti retrieved from the mice were subjected to immunohistochemistry techniques in order to ascertain protein expression and localization in IHC in the absence of Rabconnectin-3a. The proteins known to interact with Rabconnectin-3a or be of crucial importance in the hearing process at the ribbon synapse were examined. In the second aim, total protein levels will be assessed by Western Blotting (WB) techniques using whole cochlea of these mice, in order to examine the protein levels and verify the findings observed by IHC immunohistochemistry. In sum, in this project I will study the synaptic morphology and activity of IHC synapses using Rabconnectin-3a KO mice to understand the importance of Rabconnectin-3a for IHC functioning and hearing process.

Chapter II. Methods

1. Animal models

Generation of cochlea specific DMXL2 KO mice

To create these experimental mice, a Cre/lox system was used. In brief, Cre recombinase recognizes specific DNA fragment sequences known as loxP site and enables the deletion of genes that are located between these two loxP sites. Thus, to achieve a tissue specific knockout in the Cre-driver strain in which Cre recombinase is expressed by a promotor that targets specifically the cell, is created. In this particular case the promoter chosen was vGlut3 once it's found highly expressed in IHC [131].

Bearing this in mind, in the first generation a homozygous loxP-flanked mouse is mated with a Cre transgenic mouse strain in which the promoter is vGlut3. Half of the resulting offspring will be heterozygous for the loxP allele and heterozygous for the Cre transgene (**Fig.7**). In order to create the experimental mice that are going to be used in this project another mating needs to be done. So, in the second generation another homozygous loxP-flanked mouse was mated with a hemizygous Cre and heterozygous "floxed" DMXL2 (**Fig.8**).

This results in our experimental mice, IHC DMXL2 KO mice. As a control I used the WT mice (Cre transgene control). The mice used had as genetic background C57BL/6 also known as black 6.

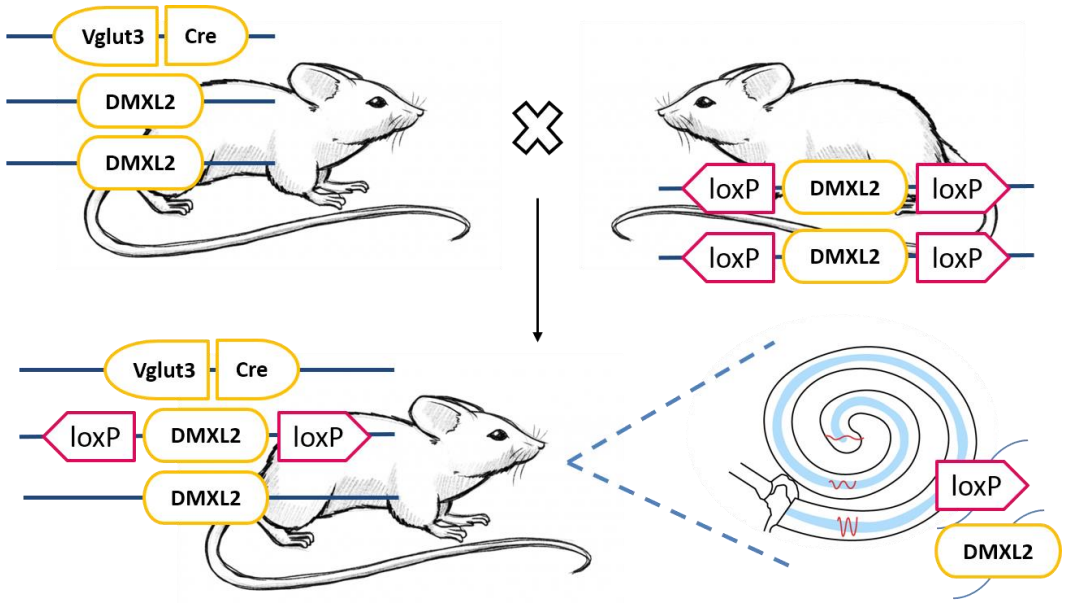

Figure 7. Cre/lox DMXL2 IHC specific KO, first generation | A Cre transgenic mouse strain is mated with a homozygous loxP-flanked mouse. In the first mating approximately 50% of the resulting offspring are heterozygous for the loxP allele and hemizygous for the Cre transgene.

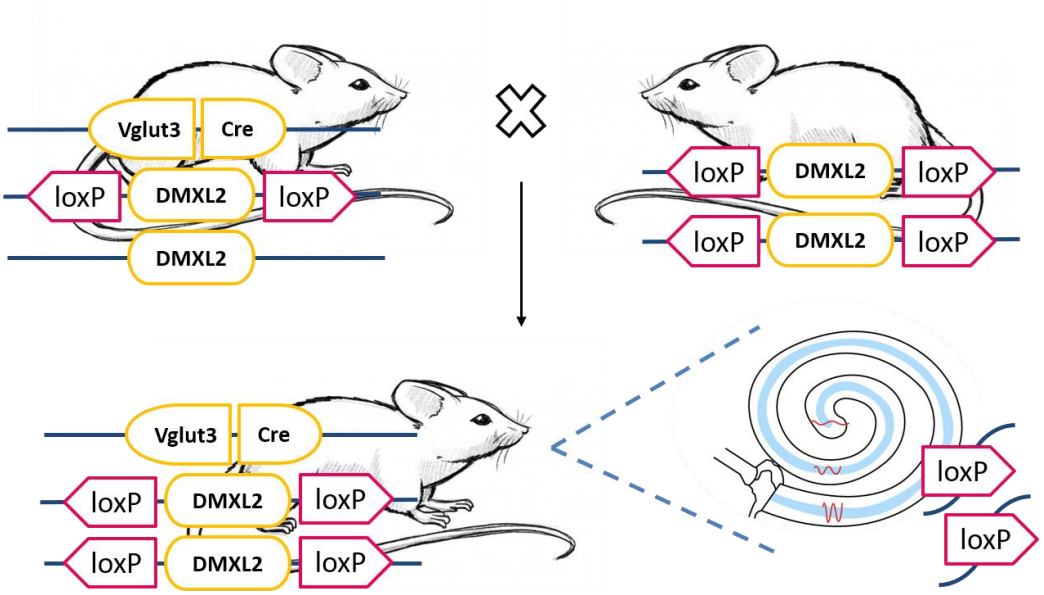

Figure 8. Cre/lox DMXL2 IHC specific KO, second generation | A hemizygous Cre heterozygous "floxed" gene is mated with a homozygous "floxed" mouse. In this second mating 25% of the offspring will be homozygous for the loxP-flanked allele and hemizygous for the Cre transgene.

All animal-related procedures were performed according to the European guidelines for animal welfare (2010/63/EU), with the explicit permission from the Niedersächsisches Landesamt für Verbraucherschutz und Lebensmittelsicherheit (LAVES), registration 15/1767. Animals were housed and bred in the Zentrale Tierexperimentelle Einrichtung (ZTE) Göttingen, with ad libitum access to water and food. Mice were kept in groups of 1–3 animals on a 12 h light/12 h dark cycle in individually ventilated cages. Both male and female animals were used for these studies at the age and genotype as indicated.

2. Cochlea dissection and preparation of total cochlea protein extracts

The mice were euthanized using a CO_2 chamber followed by cervical dislocation. The cochlea was dissected in ice cold Phosphate Buffered Saline (PBS, Sigma Life Science; Cat. No. P4417-100TAB) and immediately snapped freeze in liquid nitrogen and stored at -80ºC. A little piece of the tail of each mouse was stored at -20ºC for posterior genotyping.

To dissect the cochlea from the mice ear, the mouse was decapitated, and the head was separated by a sagittal cut in two halves. The brain was retrieved from each half using a spatula. The cochlea it's located in the bony labyrinth, this structure is the bony outer wall of the inner ear in the temporal bone. Located the structure, this one was pulled away from the rest of the mice skull and separated. Then the vestibule and the semi-circular canals were retrieved, leaving only the cochlea. This one was then collected in a tube and snap freeze in liquid nitrogen.

For total protein extraction, two cochleae per mice were transferred into a precooled 1 ml Eppendorf, tube containing 50 μl of a modified RIPA lysis buffer (50 mM Tris-HCl pH=7.5 (Roth; Cat. No. 9090); 1% (v/v) IGEPAL (Sigma Aldrich; Cat. No. 18896); 0,25 % (W/V) Na-deoxycholate (Sigma Aldrich; Cat. No. 30970); 150 mM NaCl (Roth; Cat. No. P029.3); 1 mM ethylenediamine tetraacetic acid (EDTA, Roth; Cat. No. 8040.3); 1 mM phenylmethylsulfonyl fluoride (PMSF, Roth; Cat. No. 6367,2); 1 mM NaF (Sigma Aldrich; Cat. No. S7920); PhosSTOP phosphatase inhibitors (Roche; Cat. No. 4906845001) and complete proteases inhibitors (ThermoFisher; Cat. No. 87786) and incubated for 1 hour on ice. To break and homogenize the cochlea sample a hand-held battery-operated homogenizer (VWR Pellet Mixer; Cat. No. 431-0100) was used 3 times in cycles of 1 minute of homogenization 1 minute of rest, then it was added more 50μl of modified RIPA lyses buffer and repeated the previous process of homogenization, adding more 20 μl of modified RIPA lyses buffer in the end to wash the tip of the potter in order to retrieve the maximum amount of protein possible. The sample was then set to rest 30 minutes on ice and centrifuged for 2 minutes at 4ºC at 1,000g. Finished the centrifugation, the samples were kept on a rotating wheel for 1 hour at 4ºC and centrifuged for 5 minutes at 4ºC 1,000g.

The supernatant was retrieved with a micropipette and the concentrations of the sample supernatant were determined using BCA protein determination assay (ThermoFisher; Cat. No. 23225).

3. Genotyping

3.1 Digestion of the sample and DNA precipitation

Part of the mice tail stored at -20ºC was digested in 300μl of SNET Buffer (20 mM Tris base pH=8.0, 5 mM EDTA pH=8.0, 400 mM NaCl and 0.5% SDS) and 2,5μl of Proteinase K (Roth; Cat. No. 7528,1) for 1-3 hours at 55ºC (with vortex in between). In order to precipitate the DNA present in the sample fully digested, it was added 750μl of EtOH absolute (Chemsolute, Cat. No. 2246,1) followed by the inversion of the tube and centrifugation at 11.000 g for 30 minutes. Then the supernatant was discarded, and the pellet was washed with 900μl of 70% EtOH, vortex shortly and centrifuged at 11.000 g for 20 minutes. After the centrifugation the supernatant was again discarded and 100 μl of TE buffer (10 Mm Tris-HCl pH=8.0, EDTA pH=8.0), were added to the pellet. Then the tubes were set with an open lid at 55ºC for 30- 45 minutes in the mixer. Finally, the tubes with the DNA of the mice were kept at -20ºC for posterior Polymerase Chain Reaction (PCR) reaction.

3.2 PCR reaction

For the PCR three reactions were carried out, two with the goal to observe if the mice are Cre^+ or Cre^- and the other one to assure if the mice are KO for DMXL2 or not.
For the Cre reaction there are two set of primers to reassure if the mice are Cre^+ or Cre^-, the two pair of primers used were VGLUT3-1 Oligo 13944, VGLUT3-2 13945 and Cre^+ 2 for, VGLUT3-2 rev. Bearing this in mind two mastermix were prepared following the recipe showed below:

Table 1. Reagents for the Cre PCR reaction |

5x reaction buffer	5,0 μl
MgCl2, 25 mM	2,0 μl
dNTP, 10 mM	0,5 μl
Primer set, 10 μM	0,5 μl of each primer
Dimethyl sulfoxide (DMSO, Roth; Cat. No. A994.1)	1 μl
Taq Pol (5U/μl)	0,2 μl
H_2O	14,3 μl

The reagents used are present in the Promega Go Taq ® G2 Flexi DNA (Promega, Cat. No. M7806). After preparing the mastermix, 24μl of the solution was mixed with 1μl of the mouse DNA and subjected to the following PCR program:

Table 2. PCR program for Cre reaction |

95ºC	2 min	
95ºC	45 sec	X32
55ºC	45 sec	
72ºC	1 min	
72ºC	10 min	
4ºC	∞	

For the DMXL2 reaction three primers were used: Dmxl2-5Arm, Dmxl2-3Arm and Dmxl2-LAR3. The mastermix was then prepared accordingly to the following recipe:

Table 3. Reagents for the DMXL2 PCR reaction |

5x reaction buffer	5,0 μl
MgCl2, 25 mM	4,0 μl
dNTP, 10 mM	0,5 μl
Dmxl2-5Arm, 10 μM	0,5 μl
Dmxl2-3Arm, 10 μM	0,5 μl
Dmxl2-LAR3, 10 μM	0,5 μl
Betaine 5M (Sigma Aldrich, Cat. No. B0300)	2,0 μl
Taq Pol (5U/μl)	0,25 μl
H_2O	11,25 μl

After preparing the mastermix, 24μl of the solution was mixed with 1μl of the mouse DNA and subjected to the following PCR program:

Table 4. PCR program for DMXL2 reaction |

98ºC	2 min	
98ºC	1 min	0 sec
60ºC	15 sec	X32
68ºC	1 min	
72ºC	7 min	
10ºC	∞	

3.3 Electrophoresis

In order to make the electrophoresis gel, 1,2% agarose (Biozym; Cat. No. 840004) in TAE buffer (39,95 mM Tris, 19,78 mM Acetic acid (Roth; Cat. No. 7332.3) and 5,89 mM EDTA) was prepared. Then it was mixed with 25 μl of Ethidium Bromide (VWR; Cat. No. E406-15ML) and set to rest for 30 minutes at room temperature. Then 18μl of PCR sample was loaded in the 1,2% agarose gel at 100V for 50 minutes using the Chamber Biorad DNA sub cell ™ and Biorad sub cell GT and the Electrophoresis Power Supply Consort EV231. The gel was then revealed using Intas ® UV-SYSTEME with the software GelDoc System V02.24, the ladder used was 100bp DNA ladder (Biolabs, Cat. No. N3231S).

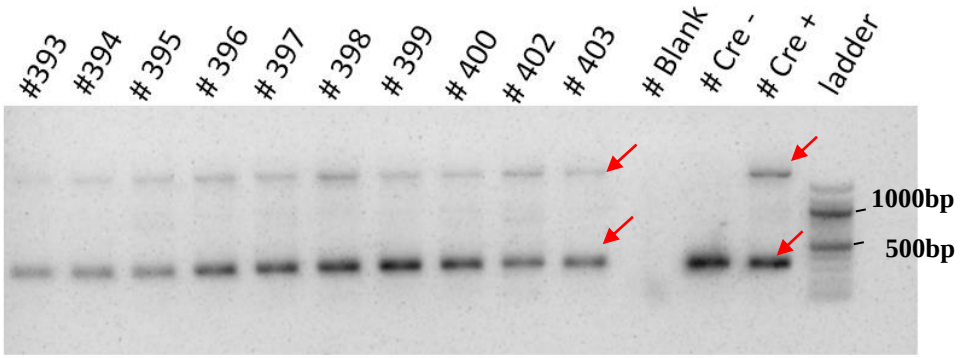

Figure 9. Eletrophoresis gel for the Cre reaction | The numbers refer to the mice identification, the Blank line is as the name refers a lane in which no mice DNA was loaded, and finally the negative control Cre^- and the positive control Cre^+. As we can see in the image all the mice subjected to the electrophoresis are Cre^+ because of the evident two bands (red arrows).

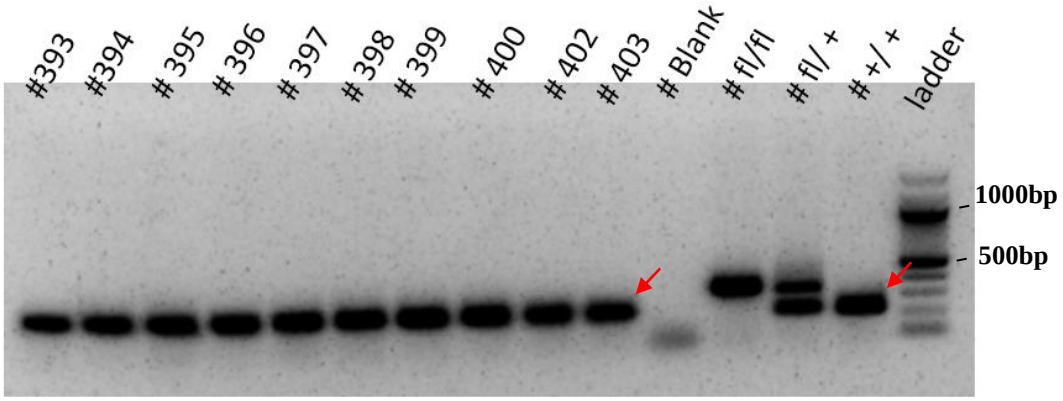

Figure 10. Eletrophoresis gel for the DMXL2 reaction | The numbers refer to the mice identification, the Blank line is as the name refers a lane in which no mice DNA was loaded, and

finally the three controls, the fl/fl which means that doesn't have the DMXL2 gene in both alelles, the fl/+ that means that is heterozygous and the +/+ that means that has the DMXL2 gene. As we can observe from the obtained results, in this gel all mice are +/+ (red arrow).

4. Western Blotting

The cochlea protein extracts samples were boiled in SDS (Sodium Dodecyl Sulfate) sample buffer (62.5 mM Tris-HCl (pH=6.8), 10% (v/v) glycerine (Roth; Cat. No. 3783.1), 2 % SDS (Roth; Cat. No. 2326.2) (w/v), 5 % (v/v) β-mercaptoethanol (Applichem; Cat. No. A1108.0250), 0,002% (w/v) brome phenol blue (Roth; Cat. No. A512.1) at 65ºC for 5 minutes to allow the denaturation of the proteins and their coating with a negative charge. Then to compare the levels of different proteins between the IHC Rabconnectin-3a KO mice with the WT, 10 μg of protein per sample were subjected to 4-15 % gradient gel (Bio Rad; Cat. No. 456-1084) or a 12% gel accordingly to the molecular weight of the set of proteins that were going to be tested. The 12% gel had a 5% stacking gel which main function is to improve electrophoresis resolution by enabling the separation of the proteins approximately at the same time. The Page ruler used was the PageRuler Plus Prestained Protein Ladder (Thermo Fisher, Cat. No. #26619) Then the electrophoresis was carried out at 90V in the BIO-RAD chamber filled with running buffer composed by 24,76 mM Tris base (Roth; Cat. No. 5429.2) 191,82 mM Glycine, (Roth; Cat. No. 3908.3) and 2,08mM SDS.

After the run the gel was transferred into Nitrocellulose Membranes (Bio Rad; Cat. No. 1620115) overnight (to assure an efficient transfer of the high molecular weight proteins), under transfer buffer (24.8 mM Tris Base, 199.81 mM glycine e 20% (V/V) methanol Roth; Cat. No. 8388,3). To decrease the unspecific binding of the primary antibodies, the membrane was incubated with 5% (W/V) milk powder (Roth; Cat. No. T145.4) in TBS-Tween20 (19,81 mM Tris, 149,90 mM NaCl and pH=7,6 and 0,1% Tween-20 (Roth; Cat. No. 9127.1); dH2O.

The primary antibodies were prepared in the blocking solution (5% (W/V) milk powder in TBS-Tween20) and let incubated overnight at 4ºC. Then three washes of ten minutes in TBS-Tween20 were carried out and the membrane was incubated with the secondary antibodies for 1 hour at room temperature.

The primary antibodies used were the following: Rabbit Anti-DMXL2 (1:500, Sigma Aldricht, Cat. No. HPA039375), Rabbit Anti-Otoferlin (1:1000, custom-prepared and available in Milosevic laboratory), rabbit Anti- ATP6V1A (1:5000, Novus Biologicals, Cat.

No. NBP1-33021), rabbit Anti- Proton ATPase (116 KDa subunit) (1:1000, Synaptic Systems, Cat. No. 109003 Polyclonal), rabbit Anti-WDR7 (1:100, Protein Tech, Cat. No. 24431-1-AP), mouse Anti-CtBP2 (1:2000, BD Transduction Laboratories, Cat. No. 612044), Rabbit Anti-Rab3a (1:1000, Synaptic Systems, Cat. No. 107 102), Rabbit Anti-vGlut3 (1:1000, Synaptic Systems, Cat. No. 135 203), and finally the loading control GAPDH (1:10 000, Sigma, Cat. No. G9545). The secondary antibodies used were Goat Anti-Rabbit (GAR) 800 (1:1000, LI-COR, Cat. No. 926-32210), Goat Anti-Rabbit (GAR) 680 (1:10 000, LI-COR, Cat. No. 926-68021) and Goat Anti-Mouse (GAM) 680 (1:10 000, LI-COR, Cat. No. 926-68020). The membrane was then revealed in Odyssey infrared imaging system (LICOR). Quantification was performed using ImageJ software.

The WB images were then analysed using ImageJ software. The inverted image of the bands was measured in every membrane and after removal of the background signal the protein levels were normalized to the loading control, GAPDH. Finally, unpaired T test was performed in order to evidence significant changes. *p value <0.05, **p value <0.01, ***p value <0.001

5. Immunohistochemistry

The cochlea was dissected in ice cold PBS. Afterwards it was fixated in 4% Formaldehyde (Sigma Aldrich; Cat. No. F8775), in PBS, for one hour in the specific case of VGlut3, DMXL2, Otoferlin, ATP6V1A and WDR7, and twenty minutes for CtBP2 and Homer. After the cochlea being fixated the organ of Corti was dissected.

The cochlea is a hollow and spiralled structure that is composed by three main chambers, the vestibular duct, tympanic duct and cochlear duct. The organ of Corti lies in the basilar membrane located in the cochlear duct. In order to access the organ of Corti the bone present in the apex of the cochlea was cautiously broken and the Reissner's membrane was carefully retrieved from the top of the organ of Corti with a tweezers. Then the apical part of the organ of Corti was withdrawal from the cochlear duct into a 12 well plate with cold PBS. Three washes of 10 minutes were carried out. Then the apical cochlear turns were incubated with Goat Serum Dilution Buffer (16% of Goat Serum (Invitrogen, Cat. No. 1395813A), 0,03% Triton X-100 (Roth, Cat. No. 3051.3), 450 mM of NaCl, 20 mM Phosphate buffer composed by 194mM sodium monohydrogen phosphate (Roth; Cat. No. 4984.1) and 46mM of sodium dihydrogen phosphate (Roth; Cat. No. T879.2) in a wet chamber at room temperature. The primary antibodies used were diluted

in Goat Serum Dilution Buffer and incubated at 4ºC overnight in a wet chamber. Thereafter, three washes of 10 minutes each were effectuated with Washing Buffer (20 mM of Phosphate Buffer, 450 mM of NaCl, 0,3% Triton X-100) at room temperature. The secondary antibodies were then diluted also in Goat Serum Dilution Buffer and the organs of Corti were incubated with them in a light protected wet chamber 1 hour at room temperature. Then, two ten-minute washes in Washing buffer were performed and the tissue was counterstained with DAPI (Roth, Cat. No. 6335,1) for 5 minutes, in a wet chamber light protected. Finally, washes were carried out with washing buffer and in 5mM Phosphate Buffer. Then the tissue was mounted on glass microscope slides (VWR; Cat. No. 631-1553) with mounting medium Mowiol (Applichem, Cat. No. A9011) and let it to dry half an hour at 37ºC.

The primary antibodies used for the immunostainings were the following: Rabbit Anti-DMXL2 (1:200, Sigma Aldricht, Cat. No. HPA039375), Mouse Anti-Otoferlin (1:200, Abcam, Cat. No. ab53233), rabbit Anti-ATP6V1A (1:100, Novus Biologicals, Cat. No. NBP1-33021), rabbit Anti-WDR7 (1:100, Protein Tech, Cat. No. 24431-1-AP), mouse Anti-CtBP2 (1:200, BD Transduction Laboratories, Cat. No. 612044), Rabbit Anti-Homer1 (1:200, Synaptic Systems, Cat. No. 160 002), Rabbit Anti-VGlut3 (1:300, Synaptic Systems, Cat. No. 135 203. The secondary antibodies used were Goat Anti-Mouse Alexa Fluor 568 (1:200, Invitrogen, Cat. No. A-11031) and Goat Anti-Rabbit Alexa Fluor 488 (1:200, Invitrogen, Cat. No. A-11034).

6. Confocal microscopy

The confocal images were acquired using a laser scanning confocal microscope, Zeiss LSM800 Laser Scanning Microscope with Airyscan 1.4 NA 63x oil immersion and 0.45 NA 10x objectives. The Z-axis stacks were acquired with a pixel size of 101.41x101.41 microns and a step size of 0.5 μm. The snaps were acquired with a pixel size of 1277.8x1277.8 microns. The images were processed and analysed using ImageJ software.

7. Data analysis

Microscopy image quantification:

The immunofluorescent images were analysed using ImageJ software. IHC ribbon synapses were manually counted in confocal z-projections of CTBP2 and Homer immunolabeled Organs of Corti. Regarding the protein quantification of otoferlin, vGlut3, V_1a, Rabconnectin-3a and Rabconnectin-3β in IHC they were semi-quantitatively accessed by the measurement of a Region of Interest (ROI) in the basal part of the IHC. The z-stack was converted into the total sum of the slices and the measurement of the mean of fluorescence intensity at the ROI in each cell was normalized to the average of the mean of fluorescent intensity values from the WT mice. Finally, an unpaired T test was performed in order to evaluate significant differences. *p value <0.05, **p value <0.01, ***p value <0.001. Intensity profile of vGlut3 and otoferlin were obtained from the average of the line scan through the cell of three single IHCs (WT and KO) at a longitudinal central plane through the nucleus from apical to basal.

Microscopy juxtaposition count:

The number of juxtaposed dots from Homer1 labelled ribbons and CtBP2 labelled ribbons for each cell was manually accessed.

Statistics

The results are presented as mean±SEM in the quantification of protein intensity in the immunofluorescence images and in the WB analysis. Statistical differences between the WT and the Rabconnectin-3a KO mice groups were accessed by unpaired Student t-test. Statistically significant differences between the two groups were labelled as * *p value* <0.05, ** *p value* <0.01 and *** *p value* <0.001.

Chapter III. Results

1. Characterization of Rabconnetin-3a expression in the mouse cochlea

To evaluate Rabconnectin-3a distribution across the organ of Corti, apical turns were immuno-labelled with anti-DMXL2 antibody (**Fig.11A**). Rabconnectin-3a was found highly expressed in IHC, and also at OHC as previously described [113] (**Fig.11B**). Rabconnectin-3a expression at the IHC was found partial throughout the cell cytoplasm and punctuated at basal area where acidifying vesicles are mostly concentrated (**Fig.11 C**). Being present in both the apical and basal region of the IHC, the plot profile (**Fig.11Di**) show a strong signal both in the apical and basal region, where synaptic vesicles are known to be enriched [70].

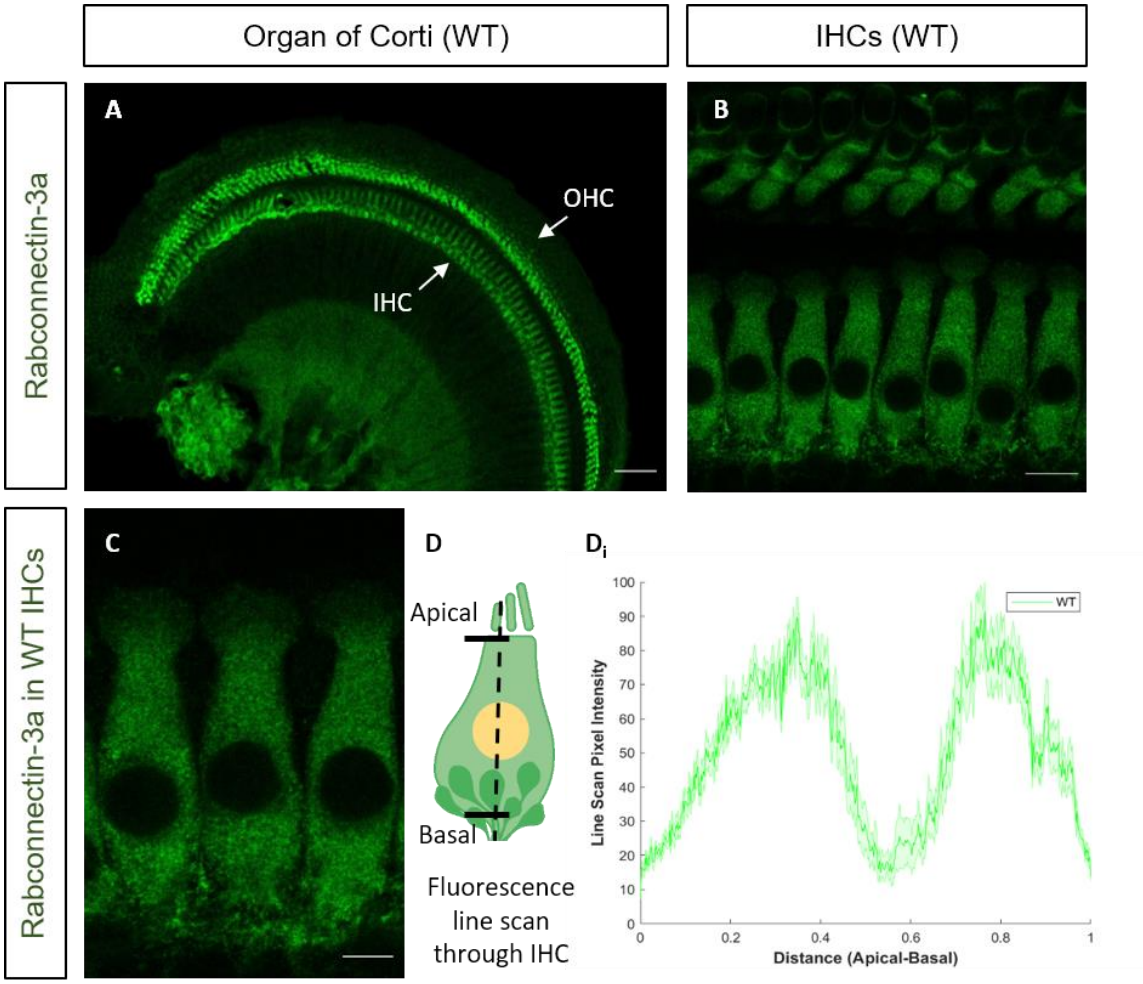

Figure 11. Rabconnectin-3a expression in IHCs| A) Z-stack section of the apical part of Rabconnectin-3a immunolabeled organ of Corti in green Scale bar 50 μm. **B) Rabconnectin-3a immunolabeled IHC and OHC, single section of a z-stack.** Scale bar 10 μm. **C) Rabconnectin-3a immunolabeled IHC, single section of a z-stack**. Scale bar 5 μm**. D) Average fluorescence intensity line profiles through the longitudinal axis of 17 IHCs from apical to basal.** Rabconnectin-3a fluorescence is present both in the apical and basal region of the IHC.

2. Verification of Rabconnectin-3a tissue-specific KO model

To better understand the role of Rabconnectin-3a at the ribbon synapse in IHC, we developed a tissue-specific Rabconnectin-3a KO mice model. Using a cre/lox system with the vGlut3 promotor region, IHCs were targeted due to higher vGlut3 expression in these cells [132] resulting in a specific DMXL2 deletion in these cells. In order to test the efficiency of Rabconnectin-3a deletion, fluorescence intensity of Rabconnectin-3a immunostaining was measured in IHC of both WT and Rabconnectin-3a KO mice. The intensity values were then normalized to the WT average. Comparatively to the WT, Rabconnectin-3a protein expression was almost absent in the IHC of the Rabconnectin-3a KO mice (**Fig.12**), showing a decrease of almost 90% at the IHCs. This result at the IHC of the KO mouse model confirms the specificity of the antibody and the efficiency of the DMXL2 gene deletion in these cells.

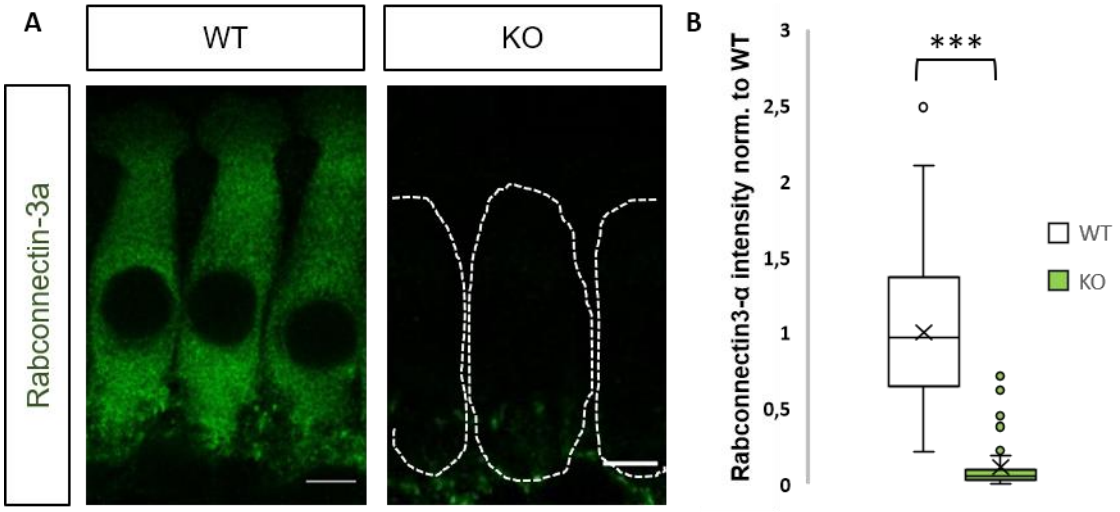

Figure 12. Rabconnectin-3a expression in WT and KO IHCs| A) Z-stack section of three Rabconnectin-3a immunolabeled IHC from WT and KO mice (P17 WT and P21 KO). In these images we can observe the absence of the protein in the KO mice. **B) Quantification of Rabconnectin-3a intensity from WT and KO mice normalized to WT average.** Rabconnectin-3a intensity levels in the KO mice are significantly decreased. WT= 6 animals (122 IHC); KO= 3 animals (58 IHC)**;** *** p value < 0.001 (unpaired Student's T test); Box plots illustrate the median with the interquartile range, whiskers indicate 10-90% of data points, and the x represents the respective mean value. Scale bar 5 μm.

To analyse the overall efficiency of DMXL2 deletion in the sensory organ of cochlea, protein extracts were prepared from KO and WT mice and subjected to immunoblotting with anti-DMXL2 antibody. Rabconnectin-3a protein levels were analysed in cochlea samples, and a 68% reduction was observed in Rabconnectin-3a IHC KO mice in comparison to WT controls (**Fig.13**). From the previous result in

Fig.11, we can argue that IHC are the main cell type contributing to this reduction but there are other cell types such as OHC that are still expressing Rabconnectin-3a. With this cre-lox KO system in the control of vGlut3 promoter we are mainly targeting IHC for DMXL2 deletion.

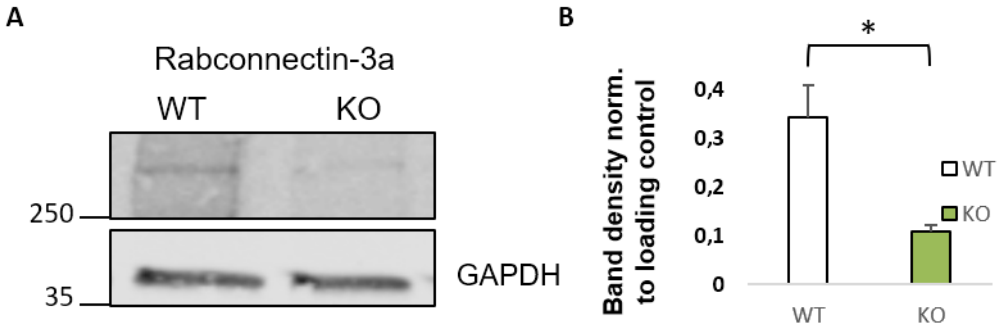

Figure 13. Rabconnectin-3a immunoblotting and quantification | A) Immunoblots showing the decrease of Rabconnectin-3a in the KO mice. B) Quantification of Rabconnectin-3a protein level. Band density quantification normalized to the housekeeping gene (GAPDH). Graphs are expressed as mean±SEM. WT = 1 animal with 3 technical replicates; KO = 2 animals with 3 technical replicates; *** p value < 0.001 (unpaired Student's T test);

3. Rabconnectin-3β expression is enriched in Rabconnectin-3a IHC KO mice

To check if the lack of Rabconnectin-3a affects the Rabconnectin-3 protein complex levels, we evaluated the Rabconnectin-3β subunit protein levels by immunohistochemistry (**Fig.14**). Mice apical turns of the organ of Corti were dissected in ice and immediately fixed in 4% formaldehyde. Rabconnectin-3β expression at the IHC from the WT mice was found partial throughout the cell cytoplasm and punctuated at basal area (**Fig.14A**) while in the IHC Rabconnectin-3a KO mice the staining was more diffused through the cell cytoplasm .Then the intensity levels of Rabconnectin-3β immunolabeled at IHC from both WT and KO mice were measured. For this measurement a ROI in the basal part of the cell was analysed, to target the region where ribbon synapses are mostly located, and all the retrieved values were normalized to the WT average.

In sum, the absence of Rabconnectin-3a resulted in a significant increase of Rabconnectin-3β at the basal area of the IHC in the KO mice in comparison to WT (**Fig.14**). This may be due, in part, to a compensatory strategy due to lack of the other subunit of the complex (Rabconnectin-3a).

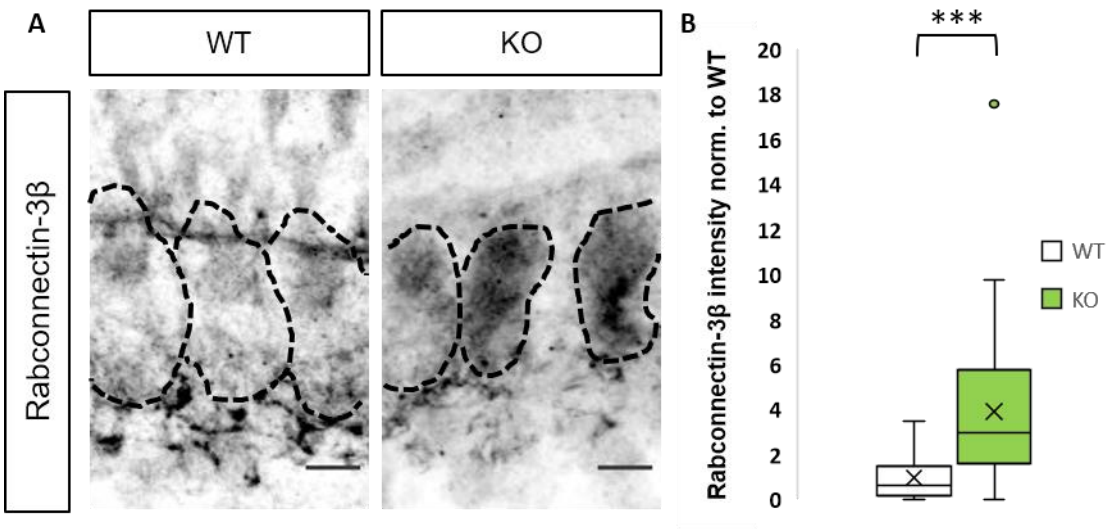

Figure 14. Rabconnectin-3β expression in WT and KO IHCs| A) Confocal maximum projection of three Rabconnectin-3β immunolabeled IHC from WT and KO mice. The IHCs are outlined at black. **B) Quantification of rabconnectin-3β mean fluorescence intensity from WT and KO mice normalized to WT average.** Rabconnectin-3β intensity levels in the KO mice are significantly increased. WT= 3 animals (57 IHC); KO= 3 animals (52 IHC)**;** *** p value < 0.001 (unpaired Student's T test); Box plots illustrate the median with the interquartile range, whiskers indicate 10-90% of data points, and the x represents the respective mean value. Scale bar 5 μm.

4. Expression of synaptic vesicle proteins Rab3 and vGlut3

Rab3a plays a role in cargo trafficking to the synapse, impairments over this type of protein could possibly lead to deficient synaptic transmission [133]. To inspect if the lack of Rabconnectin-3a in our mouse model would have a direct impact over Rab3a levels and subsequently in exocytosis, mice cochlea samples were prepared and subjected to WB technique. WB results revealed no statistical difference in the levels of Rab3a between the WT and the Rabconnectin-3a KO mice although with a tendency to be lower in the KO mice (**Fig.15**).

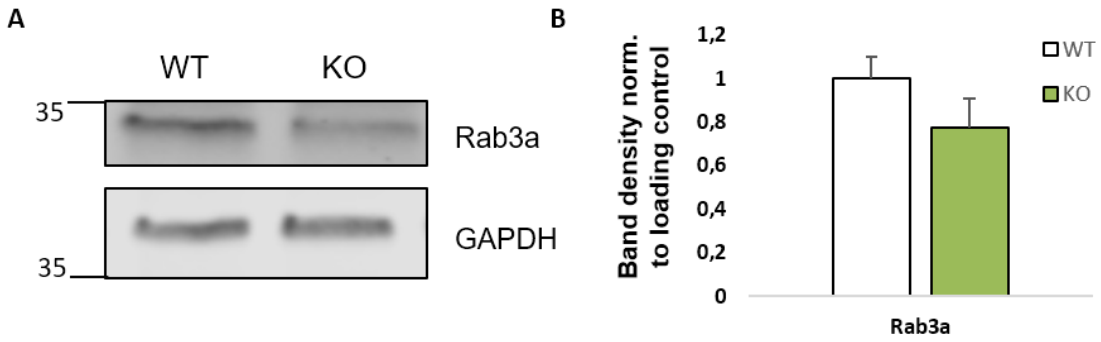

Figure 15. Rab3a protein level in mice cochleae| A) Immunoblots of Rab3a together with loading control (GAPDH). B) Quantification of Rab3a protein level. Band density quantification normalized to the housekeeping gene (GAPDH). There is no statistically significant change in protein expression level between the KO and the WT mice. Graphs are expressed as mean±SEM. WT = 9 animals; KO = 8 animals, p value > 0.05 (unpaired Student's T test);

Another protein that can give us valuable information about the nature of synaptic vesicles present in the IHC is vGlut3. This glutamate transporter is responsible for the filling of the synaptic vesicle with glutamate, being present at the vesicle's membrane [92]. vGlut3 levels were accessed by immunofluorescence technique at IHC from DMXL2 KO mice and control WT (**Fig.16**). As previously described [134] vGlut3 protein was found highly expressed in IHC cytoplasm with a higher protein expression at the basal part in the mice. Interestingly, vGlut3 showed also a very high protein level at the apical part of the IHC Rabconnectin-3a KO mice as the plot profile show in **Fig.16D**. From the measurement of the mean fluorescence intensity from the ROI in the basal region of the IHCs, we could observe a significantly increased of vGlut3 protein levels in KO mice when compared to normalized WT control. This difference can also be observed at the most basal region that probably is corresponding to the active zone where synapses are enriched. Moreover, it's observed also an enhanced apical/basal ratio of vGlut3 levels in the KO IHCs (**Fig.17**).

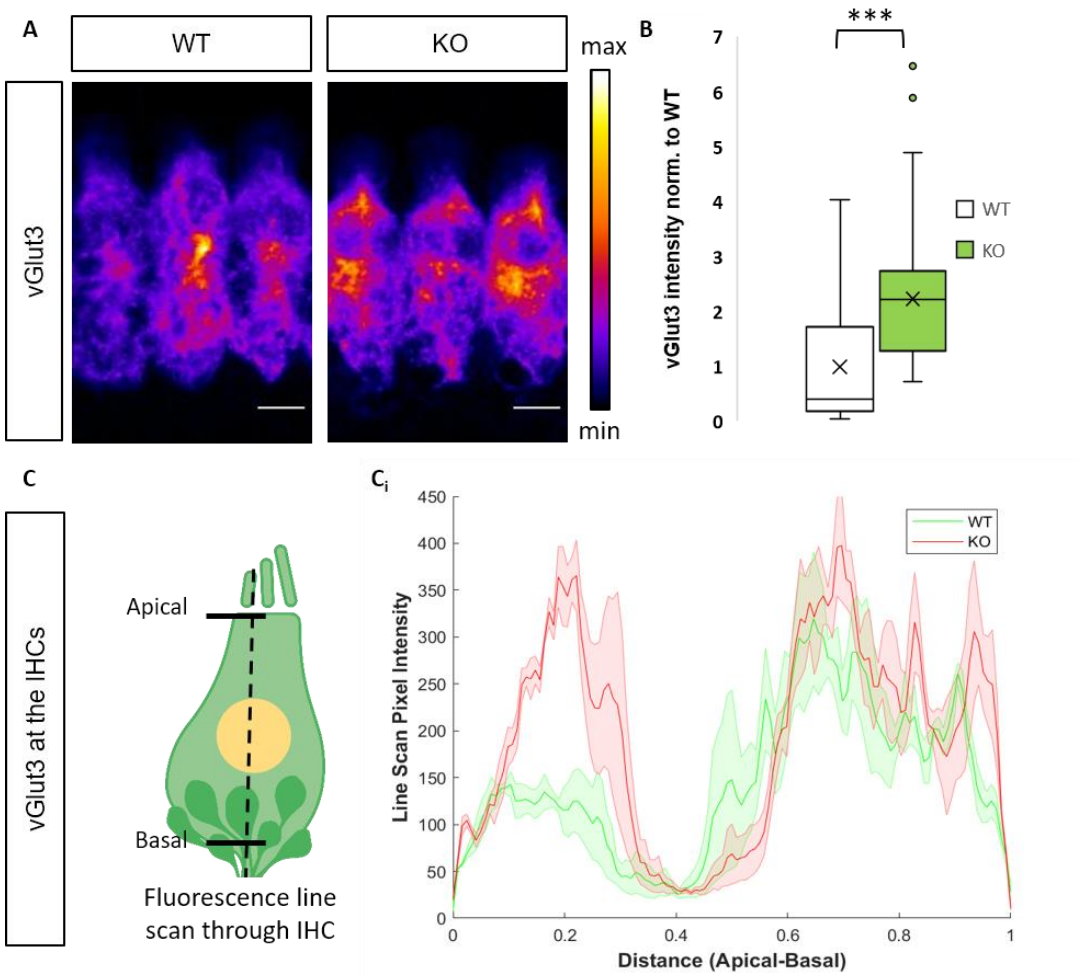

Figure 16. vGlut3 expression in WT and KO IHCs| A) Confocal maximum projection of three vGlut3 immunolabeled IHC from WT and KO mice, illustrated with an intensity-coded look-up table, calibration bar at the side. **B) Quantification of vGlut3 intensity from WT and KO mice normalized to WT average.** vGlut3 immunofluorescence intensity levels in the KO mice are significantly increased. WT= 4 animals (129 IHC); KO= 3 animals (110 IHC)**;** *** p value < 0.001 (unpaired Student's T test); Box plots illustrate the median with the interquartile range, whiskers indicate 10-90% of data points, and the x represents the respective mean value. Scale bar 5 μm. **C) vGlut3 intensity line profile.** Average of the line scan through the cell of three single IHCs (WT and KO) at a longitudinal central plane through the nucleus from apical (0.0) to basal (1.0) (n=3 cells KO and WT).

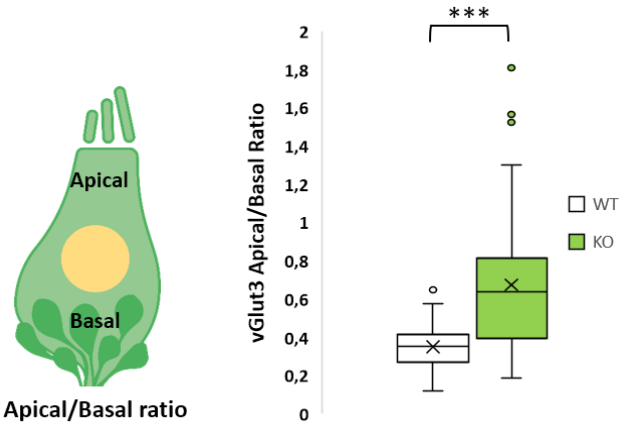

Figure 17. vGlut3 Apical/Basal ratio in WT and KO IHCs| vGlut3 Apical/Basal ratio immunofluorescence intensity levels in the KO mice are significantly increased. WT= 3 animals (35 IHC); KO= 3 animals (61 IHC)**;** *** p value < 0.001 (unpaired Student's T test); Box plots illustrate the median with the interquartile range, whiskers indicate 10-90% of data points, and the x represents the respective mean value.

vGlut3 protein levels analysis by WB from cochlea samples from KO mice and WT mice showed no statistically significant differences between the two mouse models (**Fig.18**). This may be due to the fact that in the WB technique the whole cochlea was analysed and in the immunofluorescence technique only the IHC were taken into account. vGlut3 is expressed not only in IHC but also in spiral ganglion cells (SGCs) in rat cochlea. In SGCs, vGlut3 is expressed in discrete characteristic punctate cytosolic structures present mostly in the peri-nuclear region [132].

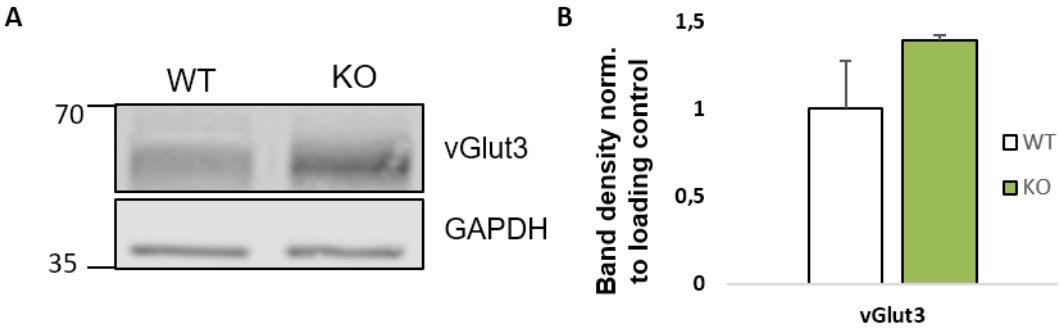

Figure 18. vGlut3 protein level in mice cochleae| A) Immunoblots of vGlut3 together with loading control (GAPDH). B) Quantification of vGlut3 protein level. Band density quantification normalized to the housekeeping gene (GAPDH). The quantification showed an increase of vGlut3 in the KO mice, however it wasn't significant. Graphs are expressed as mean±SEM. WT = 4 animals; KO = 3 animals, p value > 0.05 (unpaired Student's T test);

5. Lack of Rabconnectin-3a in IHC resulted in the decrease of V-ATPase subunits

Rabconnectin-3a was previously described as a putative regulator of V-ATPase activity [112]. Here we tested if at the specific condition of DMXL2 deletion in IHC we could also observe altered V-ATPase proteins expression and localization. Therefore, we analysed V_oa and V_1A subunits with specific antibodies. The levels of V_1A were accessed by immunohistochemistry and WB techniques. The distribution of this protein at the IHC was accessed by immunostaining and we could observe that V_1a subunit is present all through the cytoplasm in WT with higher levels at the basal part. Relatively to V_1A abundance at the IHC Rabconnectin KO mice, we could observe a significantly decreased total values of this subunit protein (**Fig.19 A, B**) being mainly absent at the basal area as the plot profile illustrate (**Fig. 19 C**). The V_1A apical/basal ratio is increased in the IHCs of the KO mice comparatively to the WT.

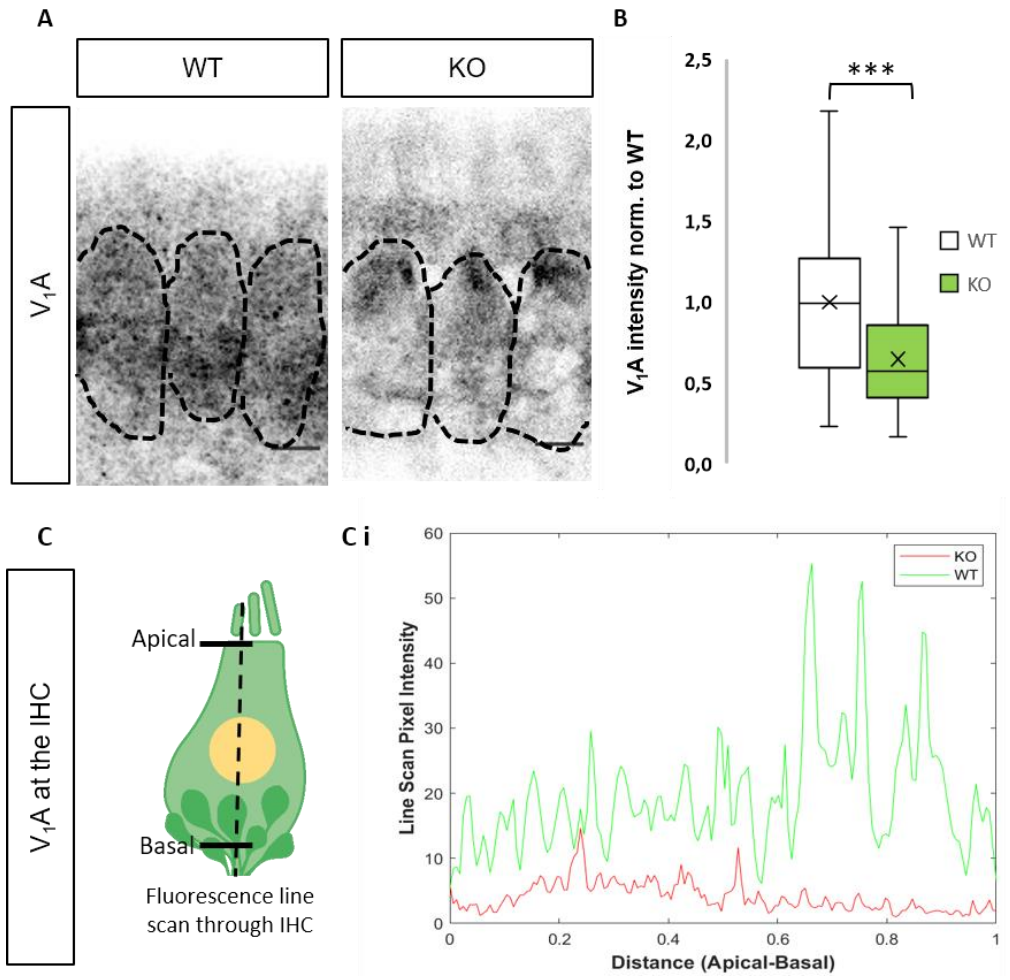

Figure 19. V_1A expression in WT and KO IHCs| A) Confocal maximum projection of three V_1a immunolabeled IHC from WT and KO mice (4 weeks WT and KO). The IHCs are outlined at black. **B) Quantification of V_1A intensity from WT and KO mice normalized to WT**

average. V_1A immunofluorescence intensity levels in the KO mice are significantly decreased. WT= 3 animals (111 IHC); KO= 3 animals (78 IHC)**; C) V_1A intensity line profile.** Average of the line scan through the cell of one single IHC (WT and KO) at a longitudinal central plane through the nucleus from apical (0.0) to basal (1.0) (n= 1 cell KO and WT). *** p value < 0.001 (unpaired Student's T test); Box plots illustrate the median with the interquartile range, whiskers indicate 10-90% of data points, and the x represents the respective mean value. Scale bar 5 μm.

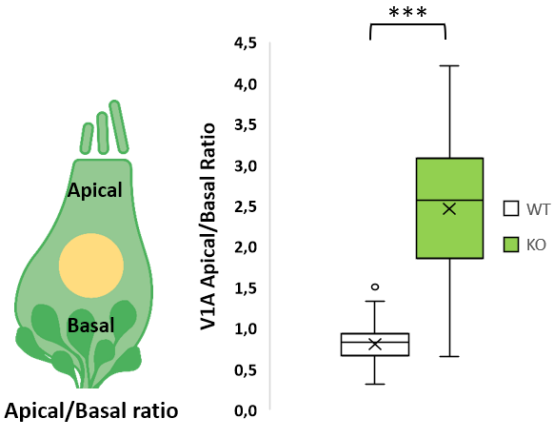

Figure 20. V_1A Apical/Basal ratio in WT and KO IHCs| V_1A Apical/Basal ratio immunofluorescence intensity levels in the KO mice are significantly increased. WT= 3 animals (51 IHC); KO= 3 animals (32 IHC)**;** *** p value < 0.001 (unpaired Student's T test); Box plots illustrate the median with the interquartile range, whiskers indicate 10-90% of data points, and the x represents the respective mean value.

Regarding V_1A subunit protein levels expression analysis from cochlea samples the results obtained from the WB technique showed no statistically significant differences between KO and WT (**Fig.21**). Observing the results, one can note a significant decrease of the V_oa subunit in KO mice in comparison to WT.

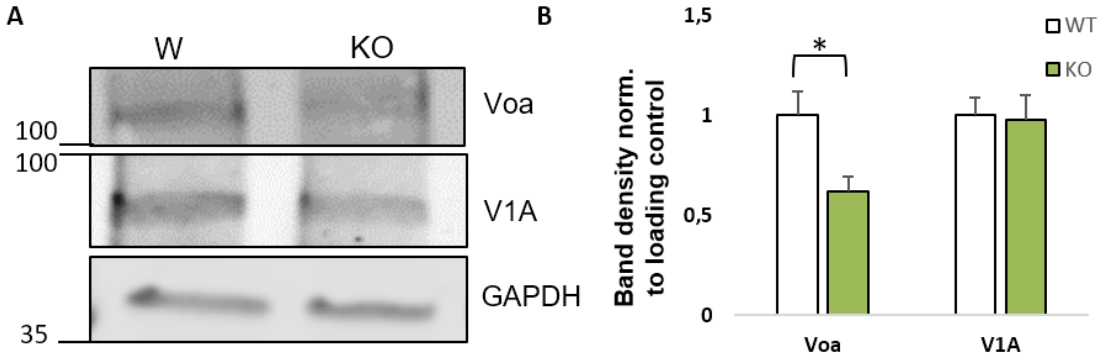

Figure 21. V_1A and V_oa protein level in mice cochlea| A) Immunoblots of Voa, V_1A together with loading control (GAPDH). B) Quantification of V_oa and V_1A protein levels. Band density quantification normalized to the housekeeping gene (GAPDH). The quantification showed significant decrease of V_oa subunit but not V_1A in the KO mice. Graphs are expressed

as mean±SEM. V_1A: WT = 9 animals; KO = 8 animals; V_oa: WT = 8 animals; KO = 7 animals, *p value < 0.05 (unpaired Student's T test);

6. Expression of the key exocytic protein, Otoferlin is significantly decreased in Rabconnectin-3a IHC KO mice

One of the key players in exocytosis is otoferlin [58]. Studies addressing the genetic insufficiency of otoferlin leading to a decrease in protein levels were found phenotypically associated with hearing impairments, or even deafness [58]. In order to detect if the lack of Rabconnectin-3a affects the level of otoferlin expression or its distribution at the IHC level, immunofluorescence technique was used (**Fig.22**). We could observe that the Otoferlin protein is expressed at the cytoplasm in WT with higher levels at the basal part. Relatively to Otoferlin distribution at the IHC Rabconnectin KO mice, we could observe a significantly decreased levels of this protein at the basal area (**Fig.22B**) as the plot profile demonstrate (**Fig.22 C_i**). A significant increase in the otoferlin apical/basal ratio was also observed in the IHC of the KO mice in comparison with the WT.

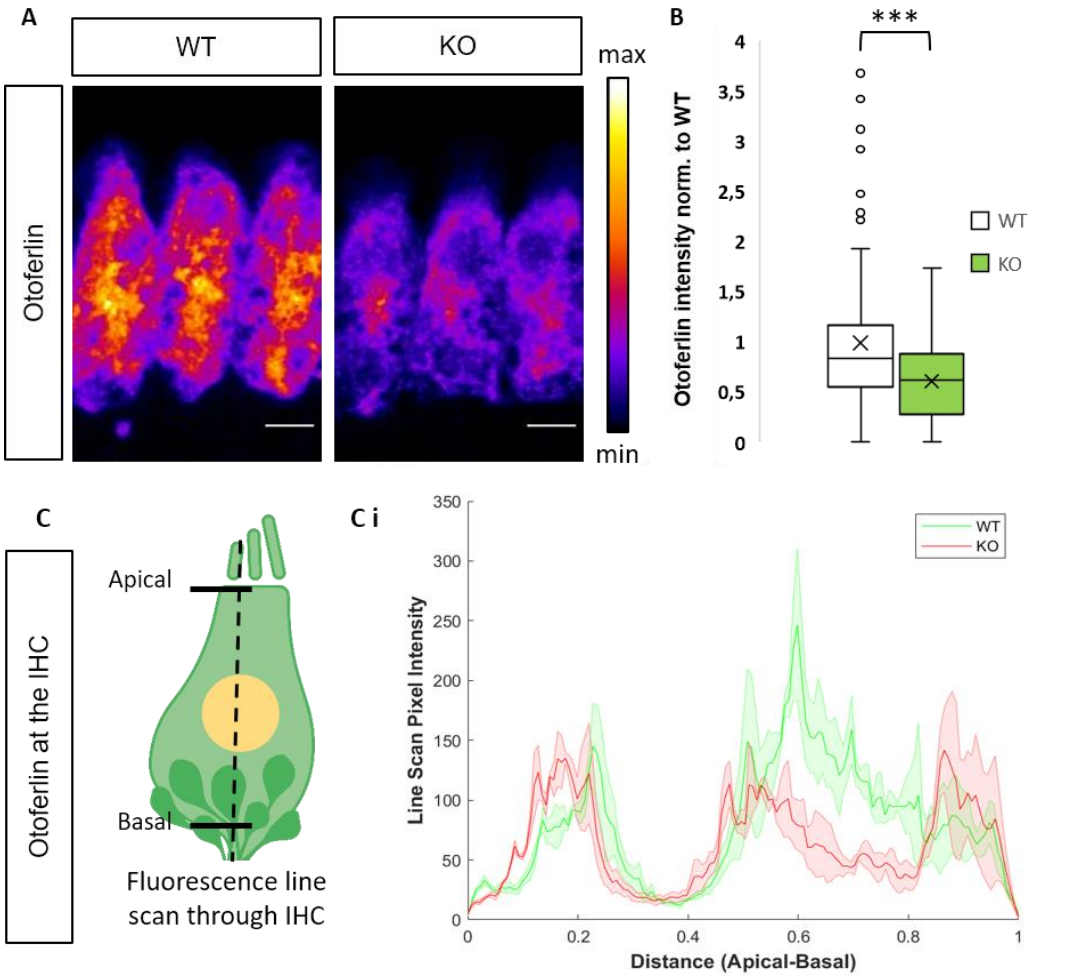

Figure 22. Otoferlin expression in WT and KO IHCs| A) Confocal maximum projection of three Otoferlin immunolabeled IHC from WT and KO mice, illustrated with an intensity-coded look-up table, calibration bar at the side. **B) Quantification of Otoferlin intensity from WT and KO mice normalized to WT average.** Otoferlin immunofluorescence intensity levels in the KO mice are significantly decreased. WT= 6 animals (124 IHC); KO= 9 animals (213 IHC)**;** *** p value < 0.001 (unpaired Student's T test); Box plots illustrate the median with the interquartile range, whiskers indicate 10-90% of data points, and the x represents the respective mean value. Scale bar 5 μm. **C) Otoferlin intensity line profile.** Average of the line scan through the cell of three single IHCs (WT and KO) at a longitudinal central plane through the nucleus from apical (0.0) to basal (1.0) (n=3 cells KO and WT).

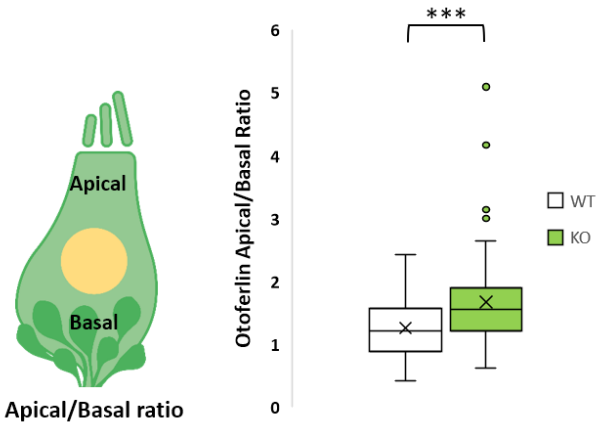

Figure 23. Otoferlin Apical/Basal ratio in WT and KO IHCs| Otoferlin Apical/Basal ratio immunofluorescence intensity levels in the KO mice are significantly increased. WT= 3 animals (63 IHC); KO= 3 animals (128 IHC)**;** *** p value < 0.001 (unpaired Student's T test); Box plots illustrate the median with the interquartile range, whiskers indicate 10-90% of data points, and the x represents the respective mean value.

In terms of total protein expression level in the IHC, Otoferlin was found significantly decreased in the Rabconnectin-3a KO mice (**Fig.24**). Reduction of 45% was obtained by the immunohistochemistry the IHC of Rabconnectin-3a KO mice in comparison to WT. When whole cochlea was analysed by WB a reduction of approximately 50% was observed in the otoferlin protein levels in Rabconnectin-3a KO mice in comparison to WT.

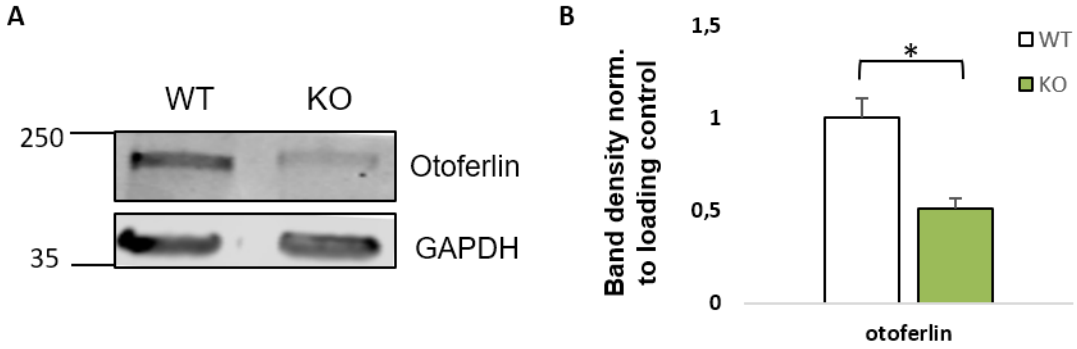

Figure 24. Otoferlin protein level in mice cochleae| A) Immunoblots of otoferlin together with loading control (GAPDH). B) Quantification of Otoferlin protein levels. Band density quantification normalized to the housekeeping gene (GAPDH). The quantification showed a significant decrease of Otoferlin in the KO mice. Graphs are expressed as mean±SEM. WT = 5 animals; KO = 4 animals, *p value < 0.05 (unpaired Student's T test);

7. Rabconnectin-3a KO mice have more ribbon synapses in IHCs

Ribbons in the IHC synapses are thought to provide rapid and indefatigable vesicular replenishment of synaptic vesicles upon stimulation. To inspect if the number of ribbon synapses varies between the WT and Rabconnectin-3a KO mice, apical turns of the organ of Corti were immunolabelled with CtBP2 (pre-synaptic zone) and Homer (post-synaptic zone). Throughout synaptic ribbon maturation both pre- and post-synaptic regions undergo several changes. Postsynaptic maturation is characterized by a transition from many small postsynaptic densities to a single larger one. Meanwhile presynaptic maturation is characterized by the fusion of ribbon precursors at the active zone which translates into a ribbon number decrease [51]. To inspect the colocalization of presynaptic (CtBP2) and postsynaptic (Homer) markers the colocalization of the two probes was accessed. Visually the two probes overlapped almost perfectly: As we can see in the below image these two proteins colocalize (**Fig.25**). The Pearson correlation coefficient presented was 0.35 for WT and 0.33 for KO suggesting prominent colocalization of the two probes.

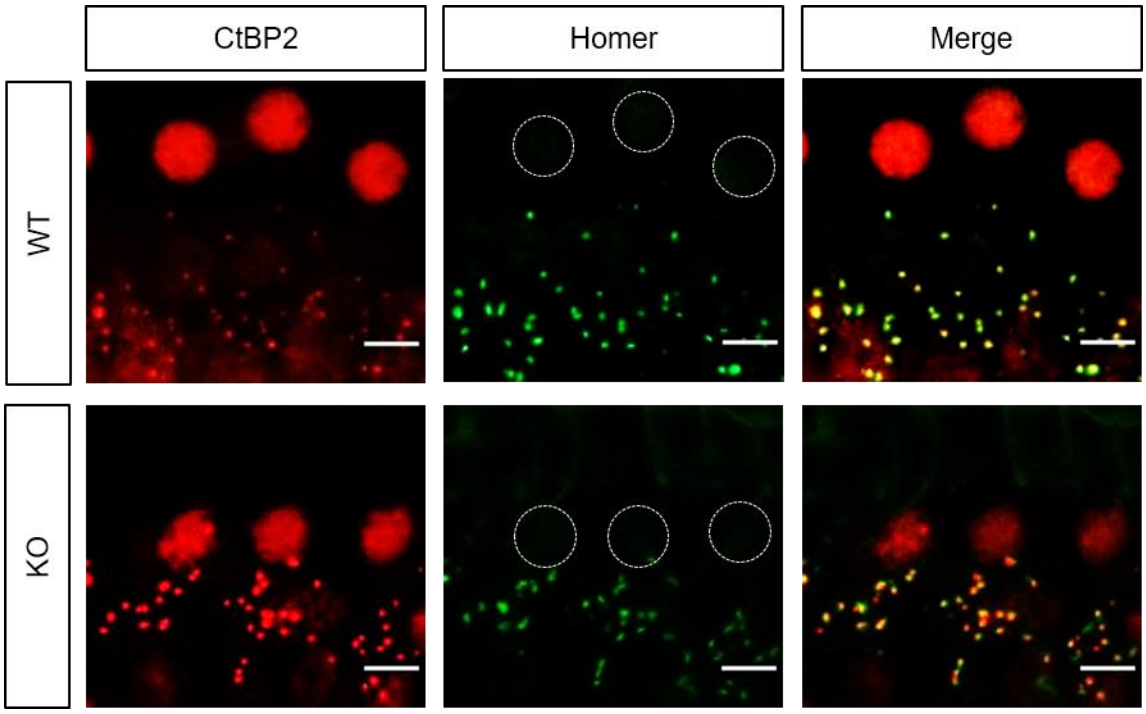

Figure 25. Confocal maximum projections of Homer and CtBP2 labelled ribbons | CtBP2 (in red) immunostaining results not only in the marking of the ribbon but also in the marking of the nucleus of the IHC. CtBP2 is present in the presynaptic ribbon body while Homer (in green) is present in the postsynaptic ribbon body. In the WT panel, four IHC are showed while in the KO mice there are three. The number of animals used to ascertain the Pearson Correlation

coefficient were WT n= 57 IHC from 3 animals; KO n=52 IHC from 3 animals**;** IHC nucleus are outlined in white circles in Homer staining images. Scale bar 5 μm.

Then the number of punctate structures per IHC was manually accessed. The quantification of these two proteins presented a higher count of CtBP2/Homer juxtaposed structures in the Rabconnectin-3a KO mice (juxtaposed CtBP2 and Homer structures 8,82±0,37 for WT mice and 12,07±0,33 or the KO mice). The number of CtBP2 and Homer labelled ribbons presented also a higher count in the Rabconnectin-3a KO mice (**Fig.26**), (Homer: 13,07±0,41 for KO mice and 11,30±0,41 for WT mice; CtBP2: 13,60±0,40 for KO mice and 11,70±0,36 for WT mice; values are expressed as mean±SEM).

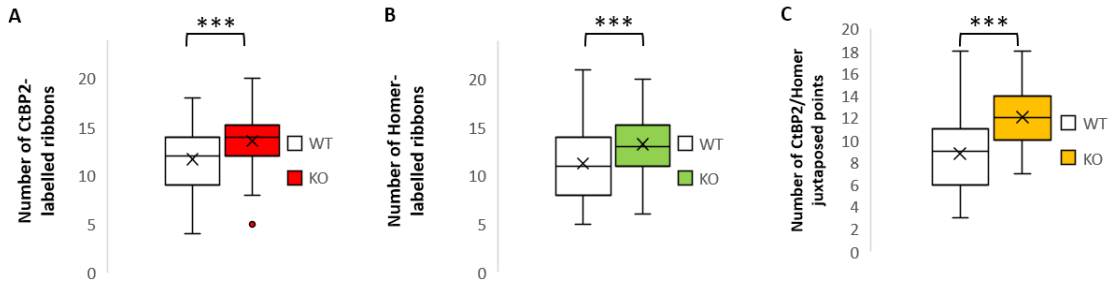

Figure 26. CtBP2 and Homer labelled ribbons quantification| A) Quantification of CtBP2-labelled ribbons. CTBP2 labelled ribbons numbers were found increased in the KO mice (n=57 IHC from 3 animals) in comparison to WT (n=52 IHC from 3 animals)**. B) Quantification of Homer-labelled ribbons.** Homer-labelled ribbons numbers were found increased in the KO mice (n=52 IHC from 3 animals) in comparison to WT (n=57 IHC from 3 animals); **C) Quantification of CtBP2 and Homer juxtaposed punctate structures.** The number of CtBP2 and Homer juxtaposed punctuated structures presented a higher number in the KO mice. The *** p value < 0.001 (unpaired Student's T test); Box plots illustrate the median with the interquartile range, whiskers indicate 10-90% of data points, and the x represents the respective mean value.

Chapter IV. Discussion

Discussion

Characterization of Rabconnectin-3a expression in the mouse cochlea

Results from the characterization of Rabconnectin-3a protein levels in the organ of Corti by immunofluorescence showed that this protein is highly expressed in the IHC of the WT mice and at lower extent at OHC. Although DMXL2 was suggested to be expressed in IHC, OHC and spiral ganglion cells, results here suggest that they are enriched in the IHC. An enrichment in the IHC over OHC suggests that Rabconnectin-3a likely affects sound encoding through synaptic function in IHC compared to modulatory function of OHC, but this remains to be tested in future.

Moreover, Rabconnectin-3a protein distribution in the IHC overlaps with other proteins, for example a big similarity with vGlut3 protein expression can be evidenced [134]. To some extent, this is expected since both proteins are associated with synaptic vesicles [106], [55].

In the KO mice we obtained almost a complete deletion of Rabconnectin-3a expression at IHCs (KO higher than 90%) while results from WB showed a reduction around 68% in rabconnectin-3a protein levels in total cochlea sample of KO mice in comparison to WT. This reduction suggests that only a small fraction of the cochlear cells are lacking DMXL2 expression. In fact, IHC are a small fraction of the cochlear cells and showed very high Rabconnectin-3a basal expression levels by immunostaining with anti-DMXL2 antibody (**Fig.11**). So, we can argue that IHCs lacking Rabconnectin-3a protein in the KO mouse model are the main reason for the reduction observed at the total protein level in the whole cochlea of KO mice. This also emphasizes the importance of tissue specific removal of a protein of interest to study their role in a particular behaviour. Using a vGlut3-cre line, here we were able to achieve an IHC specific KO of rabconnectin-3a to understand its function in this cell type.

Rabconnectin-3β is increased and V-ATPase are decreased in the Rabconnectin-3a IHC KO mice

The decrease of Rabconnectin-3a resulted in the increase of Rabconnectin3-β. Rabconnectin-3 complex is constituted by these two subunits. One can suggest a compensation mechanism between the two subunits, when one subunit is decreased it is verified an increase of the other counterpart. The function of rabconnectin-3β in IHC

function is not known yet, and it would be interesting to check if both the proteins participate in the same pathway to affect the IHC function.

Regarding the regulatory role in the V-ATPase proton pump, Rabconnectin-3a absence resulted in the decrease of both cytosolic, V_1A, and membrane, V_oa, units at IHC basal region of the Rabconnectin-3a KO mice. This can suggest a regulatory role of rabconnectin-3 complex, wherein they control the assembly of V-ATPase complex. While in the zebra fish IHC, both the assembly and acidification of the hair cells were affected, absence of rabconnectin-3a only affects trafficking but not the functionality of endosomes in the zebrafish NC cells. It would be interesting to test further if in the absence of rabconnectin-3a, only the assembly of V-ATPase complex is affected in the mammalian IHC or also the functioning of the proton pump. Is so, it is also expected that along with these changes, we would obtain similar impairment in acidification of vesicles as evidenced in previous mutant zebrafish model, although this experiment was not addressed here and needed further confirmation.

vGlut3 is increased in the KO mice while trafficking remains unchanged

Another interesting result was the increase of vGlut3 expression at IHC of our Rabconnectin-3a IHC KO mice. vGlut3 is an important transporter that is responsible for the uptake of the glutamate neurotransmitter into the synaptic vesicles, being considered as an essential component for synaptic transmission and hearing [55], [57]. Comparatively to the zebrafish mutant, where the protein levels of vGlut3 were not significantly changed, we found a significant increase at the protein levels at the IHC lacking Rabconnectin-3a. Although only a tendency was observed at the total protein level, but not a significant increase, it would be interesting to further test whether it is only a change in distribution of vGlut3. It would also be worthy to check if there is an increase of vGlut3 at the transcript level. If rabconnectin-3a indeed affects V-ATPase function and driving force of neurotransmitter uptake is reduced, an increase in vGlut3 could be a compensatory mechanism adapted by the IHC. In terms of synaptic vesicle trafficking, we could not find any significant differences in rab3a protein expression at whole cochlea WB between WT and KO mice. Taken together, the results suggest that these mice have normal transport of synaptic vesicles and docking at the active zone. Although we need to further address Rab3a protein levels specifically at IHC by immunofluorescence.

Otoferlin is reduced in rabconnectin-3a IHC KO mice

Nothing is known about a possible interaction between Rabconnectin-3a and otoferlin. Otoferlin is a known specific marker for labelling IHC since this protein is constitutively highly expressed in these cells [135]. The results obtained by the immunofluorescence technique evidenced a significant decrease (reduction of 45%) of otoferlin protein levels at IHCs of our rabconnectin-3a IHC KO mice.

Otoferlin is essential for functional exocytosis in both auditory and vestibular hair cells [58], [81]. In an otoferlin mutant mice exocytosis was abolished which resulted in hearing impairments, however, interestingly, the calcium currents as well as the morphology of the ribbon synapses did not present any changes [58]. Thus, otoferlin is hypothesized as the main calcium sensor in IHC synaptic transmission, triggering synaptic vesicle fusion with the membrane in the IHC active zone [58]. Additionally, it was also proposed that this protein play an important role in synaptic vesicle pool replenishment in the IHC of a otoferlin mutant mice [44]. Otoferlin protein reductions were evidenced in hair cells of the inner ear of mutant *pwi* zebrafish, with disrupted *wrb* (TRC40 receptor tryptophan-rich basic protein) [136].These zebrafish presented also hearing impairments, a result of otoferlin decrease [137]. The TRC40 pathway mediates tail-anchored proteins such as otoferlin into membranes and it's essential for assuring sufficient otoferlin biogenesis [138].

Rabconnectin-3a and β were shown to form a complex with Cav2.1 and Cav2.2 channels in mouse brain, both subunits being responsible for Cav2.2 current density. This regulation could lead to the hypothesis that Rabconnectin complex regulates brain function by controlling calcium influx [116]. We can speculate that the lack of Rabconnectin-3a would lead to a decrease in the calcium influx into the IHC and consequently to a reduction in otoferlin levels that ultimately is linked to a deficient exocytosis [58]. It remains to be tested if absence of Rabconnectin-3a affects exocytosis, especially given the observed downregulation in otoferlin levels, it would be important to check vesicle fusion and pool replenishment in the KO IHC in future.

Additionally, the significant decrease of otoferlin protein in the Rabconnectin-3a IHC KO mice can suggest that these two proteins could be indirectly interacting with each other. Another suggestion would be that Rabconnectin-3a is somehow involved in TCR40 pathway and its absence can result in otoferlin reduction, however this hypothesis needs further study.

CtBP2 and Homer levels are increased in rabconnectin-3a IHC KO mice

Rabconnectin-3a is significantly decreased in the IHC of the KO mice model, specially from the analyses of the immunofluorescence images, one can affirm that this protein is even absent in the IHC. Some studies conducted in both humans [113] and Rabconnectin-3a mutant zebrafish [112] linked mutations in Rabconnectin-3a gene to the phenotype of hearing impairment. Regarding the zebrafish study, no changes in both pre and post synaptic proteins were spotted, both proteins MAGUK and Ribeye b presented puncta with similar colocalization between the WT and mutant zebrafish. Additionally, no drastic morphological changes nor cell death was evidenced [112]. Interestingly, here in our Rabconnectin-3a IHC KO mice model, changes in pre and post synaptic proteins were spotted. Both Homer and CtBP2 were significantly increased in the KO model. Thus, showing that the KO mice had more ribbons comparatively to the WT. This can be further tested by a detailed morphological analysis using electron microscopy in future.

Fusion of ribbon precursors is a critical step in IHC presynaptic active zone maturation and can determine the synaptic vesicle tethering ability [51]. Throughout the developmental stage of the IHC synapse, the fusion of floating ribbon precursors contributes to the reduction of ribbon numbers while controlling ribbon size and assuring synaptic confinement [51]. Interestingly, previous studies suggested that the rabconnectin3 complex would play a role in the synaptic development of the lateral line due to the requirement of this complex to process the intracellular domain of Notch in other organisms and cell types [114], [111]. We can hypothesize that the increased number of ribbons observed in our Rabconnectin-3a IHC KO mice can be due to impairments in this crucial step of maturation by the lack of Rabconnectin-3a. Nevertheless, additional experiments need to be made in order to confirm if the increasing numbers of ribbons is a result of a defect in the maturation process.

Chapter V. Conclusion and Future Work

Conclusion and Future Work

Rabconnectin-3a is involved in synaptic transmission at IHC. The mechanisms behind its involvement are still not clear but it is suggested that it may play a modulatory role in the acidification of the synaptic vesicles. In this project it was shown that Rabconnectin-3a absence in Rabconnectin-3a IHC KO mice results in significant changes in V-ATPase subunits expression at the IHC. This decrease may affect synaptic vesicle acidification and ultimately synaptic transmission at the IHC. These results are in line with a previous study made in Rabconnectin-3a zebrafish mutant; in both studies, the lack of Rabconnectin-3a affected directly V-ATPase localization and consequently synaptic vesicle acidification. To verify if our KO model has similar acidification deficit, the lysotracker dye assay could be used to measure the pH levels at the synaptic vesicles and compare them between the KO and WT mice. In the future, it would be also interesting to investigate the glutamate levels at the IHC of our KO model since the V-ATPase impairment could consequently lead to a deficient uptake and filling of glutamate by the synaptic vesicle.

Otoferlin, a known key player in exocytosis was also found decreased in IHC of our Rabconncetin-3a IHC KO mouse model. This may suggest an interaction between Rabconnectin-3a and Otoferlin. To test this hypothesis, immunoprecipitation assays could be performed. In previous work performed in Rabconnectin-3a mutant zebrafish the protein Otoferlin was not evaluated, so it would also be interesting to investigate if that Knock-in DMXL2 mutant model altered Otoferlin levels would also be observed at the IHC. To verify if the lack of Rabconnectin-3a affects otoferlin protein expression, it would be important to access the levels of some proteins involved in TRC40 pathway at IHC. On the other hand, this decrease could also be a result of developmental impairments of the ribbon synapse, so it would be interesting the evaluation of synaptogamins levels in both WT and KO mice.

To study the vesicle trafficking and number, the proteins rab3a and vGlut3 levels at the whole cochlea were accessed. And contrarily with previous results, there was a significant change in the vGlut3 protein. vGlut3 was increased in the Rabconnectin-3a IHC KO mice. On the other hand, rab3a levels were not changed which is following previous results of the rabconnectin-3a mutant zebrafish.

The ribbon number was increased, which may imply a maturation step impairment. One of the maturation steps that the ribbon synapse undergoes is ribbon fusion, which results in the reduction of ribbon number. To address this hypothesis, it would be interesting to perform electron microscopy analysis to study the ribbon morphology between the IHC from WT and Rabconnectin-3a KO mice.

In conclusion, new insights in the hearing process were obtained during this study where the role of Rabconnectin-3a in IHC ribbon synapse was addressed. Our unique mouse model generated and here studied offers an opportunity to elucidate how previous mutations in DMXL2 gene affecting Rabconnectin-3a protein expression can lead to hearing loss and deafness in humans.

Chapter VI. References

[1] Z. Qing and D. Mao-li, “Anatomy and physiology of peripheral auditory system and commen causes of hearing loss,” *J. Otol.*, vol. 4, no. 1, pp. 7–14, Jun. 2009.

[2] R. Fettiplace, “Hair Cell Transduction, Tuning, and Synaptic Transmission in the Mammalian Cochlea,” in *Comprehensive Physiology*, vol. 205, no. 4967, Hoboken, NJ, USA: John Wiley & Sons, Inc., 2017, pp. 1197–1227.

[3] D. R. McPherson, “Sensory Hair Cells: An Introduction to Structure and Physiology,” *Integr. Comp. Biol.*, vol. 58, no. 2, pp. 282–300, Aug. 2018.

[4] *CUMMINGS OTOLARYNGOLOGY - INTERNATIONAL EDITION : head and neck surgery, 3.* ELSEVIER - HEALTH SCIENCE, 2020.

[5] H. W. Francis, A. Rivas, M. Lehar, and D. K. Ryugo, “Two types of afferent terminals innervate cochlear inner hair cells in C57BL/6J mice,” *Brain Res.*, vol. 1016, no. 2, pp. 182–194, Aug. 2004.

[6] S. S. Spicer, G. N. Thomopoulos, and B. A. Schulte, “Novel membranous structures in apical and basal compartments of inner hair cells,” *J. Comp. Neurol.*, vol. 409, no. 3, pp. 424–437, Jul. 1999.

[7] A. Bullen *et al.*, “Association of intracellular and synaptic organization in cochlear inner hair cells revealed by 3D electron microscopy,” *J. Cell Sci.*, vol. 128, no. 14, pp. 2529–2540, Jul. 2015.

[8] C. Wichmann and T. Moser, “Relating structure and function of inner hair cell ribbon synapses,” *Cell and Tissue Research*, vol. 361, no. 1. Springer Verlag, pp. 95–114, 02-Jul-2015.

[9] R. G. Zhai and H. J. Bellen, “The architecture of the active zone in the presynaptic nerve terminal,” *Physiology*, vol. 19, no. 5. American Physiological Society, pp. 262–270, Oct-2004.

[10] N. Kiang, *Discharge patterns of single fibers in the cat’s auditory nerve.* Cambridge Mass.: M.I.T. Press, 1965.

[11] J. E. Rose, J. F. Brugge, D. J. Anderson, and J. E. Hind, “Phase-locked response to low-frequency tones in single auditory nerve fibers of the squirrel monkey.,” *J. Neurophysiol.*, vol. 30, no. 4, pp. 769–793, 1967.

[12] A. R. Palmer and I. J. Russell, “Phase-locking in the cochlear nerve of the guinea-pig and its relation to the receptor potential of inner hair-cells,” *Hear. Res.*, vol. 24, no. 1, pp. 1–15, 1986.

[13] C. Köppl, “Phase Locking to High Frequencies in the Auditory Nerve and Cochlear Nucleus Magnocellularis of the Barn Owl, Tyto alba,” *J. Neurosci.*, vol. 17, no. 9, pp. 3312–3321, May 1997.

[14] J. D. Goutman, “Transmitter release from cochlear hair cells is phase locked to cyclic stimuli of different intensities and frequencies,” *J. Neurosci.*, vol. 32, no. 47, pp. 17025–17036, Nov. 2012.

[15] G. L. Li, S. Cho, and H. von Gersdorff, “Phase-locking precision is enhanced by multiquantal release at an auditory hair cell ribbon synapse,” *Neuron*, vol. 83, no. 6, pp.

1404–1417, 2014.

[16] J. Platzer *et al.*, “Congenital deafness and sinoatrial node dysfunction in mice lacking class D L-type Ca2+ channels,” *Cell*, vol. 102, no. 1, pp. 89–97, Jul. 2000.

[17] A. Brandt, J. Striessnig, and T. Moser, “Cav1.3 Channels Are Essential for Development and Presynaptic Activity of Cochlear Inner Hair Cells,” *J. Neurosci.*, vol. 23, no. 34, pp. 10832–10840, Nov. 2003.

[18] A. Brandt, D. Khimich, and T. Moser, “Few CaV1.3 channels regulate the exocytosis of a synaptic vesicle at the hair cell ribbon synapse,” *J. Neurosci.*, vol. 25, no. 50, pp. 11577–11585, Dec. 2005.

[19] W. M. Roberts, R. A. Jacobs, and A. J. Hudspeth, “Colocalization of ion channels involved in frequency selectivity and synaptic transmission at presynaptic active zones of hair cells,” *J. Neurosci.*, vol. 10, no. 11, pp. 3664–3684, 1990.

[20] A. Rodriguez-Contreras and E. N. Yamoah, “Direct measurement of single-channel Ca2+ currents in bullfrog hair cells reveals two distinct channel subtypes,” *J. Physiol.*, vol. 534, no. 3, pp. 669–689, Aug. 2001.

[21] N. P. Issa and A. J. Hudspeth, “Clustering of Ca2+ channels and Ca2+-activated K+ channels at fluorescently labeled presynaptic active zones of hair cells,” *Proc. Natl. Acad. Sci. U. S. A.*, vol. 91, no. 16, pp. 7578–7582, Aug. 1994.

[22] T. Tucker and R. Fettiplace, “Confocal imaging of calcium microdomains and calcium extrusion in turtle hair cells.,” *Neuron*, vol. 15, no. 6, pp. 1323–35, Dec. 1995.

[23] D. Zenisek, V. Davila, L. Wan, and W. Almers, “Imaging calcium entry sites and ribbon structures in two presynaptic cells,” *J. Neurosci.*, vol. 23, no. 7, pp. 2538–2548, Apr. 2003.

[24] S. Sidi, E. Busch-Nentwich, R. Friedrich, U. Schoenberger, and T. Nicolson, “gemini Encodes a Zebrafish L-Type Calcium Channel That Localizes at Sensory Hair Cell Ribbon Synapses,” *J. Neurosci.*, vol. 24, no. 17, pp. 4213–4223, Apr. 2004.

[25] R. Nouvian, D. Beutner, T. D. Parsons, and T. Moser, “Structure and function of the hair cell ribbon synapse,” *Journal of Membrane Biology*, vol. 209, no. 2–3. Springer, pp. 153–165, Jan-2006.

[26] H. M. Sobkowicz, J. E. Rose, G. E. Scott, and S. M. Slapnick, “Ribbon synapses in the developing intact and cultured organ of corti in the mouse,” *J. Neurosci.*, vol. 2, no. 7, pp. 942–957, 1982.

[27] D. Khimich *et al.*, “Hair cell synaptic ribbons are essential for synchronous auditory signalling,” *Nature*, vol. 434, no. 7035, pp. 889–894, Apr. 2005.

[28] F. Schmitz, A. Königstorfer, and T. C. Südhof, “RIBEYE, a component of synaptic ribbons: A protein’s journey through evolution provides insight into synaptic ribbon function,” *Neuron*, vol. 28, no. 3, pp. 857–872, 2000.

[29] F. Schmitz, “The making of synaptic ribbons: How they are built and what they do,” *Neuroscientist*, vol. 15, no. 6. pp. 611–624, Dec-2009.

[30] O. Dick, I. Hack, W. D. Altrock, C. C. Garner, E. D. Gundelfinger, and J. H. Brandsttter,

"Localization of the presynaptic cytomatrix protein Piccolo at ribbon and conventional synapses in the rat retina: Comparison with Bassoon," *J. Comp. Neurol.*, vol. 439, no. 2, pp. 224–234, Oct. 2001.

[31] O. Dick *et al.*, "The presynaptic active zone protein bassoon is essential for photoreceptor ribbon synapse formation in the retina," *Neuron*, vol. 37, no. 5, pp. 775–786, Mar. 2003.

[32] H. Regus-Leidig *et al.*, "Identification and Immunocytochemical Characterization of Piccolino, a Novel Piccolo Splice Variant Selectively Expressed at Sensory Ribbon Synapses of the Eye and Ear," *PLoS One*, vol. 8, no. 8, Aug. 2013.

[33] H. Regus-Leidig *et al.*, "In vivo knockdown of Piccolino disrupts presynaptic ribbon morphology in mouse photoreceptor synapses," *Front. Cell. Neurosci.*, vol. 8, no. SEP, p. 259, Sep. 2014.

[34] T. Frank *et al.*, "Bassoon and the synaptic ribbon organize Ca2+ channels and vesicles to add release sites and promote refilling," *Neuron*, vol. 68, no. 4, pp. 724–738, Nov. 2010.

[35] A. H. Bunt, "Enzymatic digestion of synaptic ribbons in amphibian retinal photoreceptors," *Brain Res.*, vol. 25, no. 3, pp. 571–577, Feb. 1971.

[36] E. G. Gray and H. L. Pease, "On understanding the organisation of the retinal receptor synapses," *Brain Res.*, vol. 35, no. 1, pp. 1–15, Dec. 1971.

[37] L. Vollrath and I. Spiwoks-Becker, "Plasticity of retinal ribbon synapses.," *Microsc. Res. Tech.*, vol. 35, no. 6, pp. 472–87, Dec. 1996.

[38] D. Lenzi and H. Von Gersdorff, "Structure suggests function: The case for synaptic ribbons as exocytotic nanomachines," *BioEssays*, vol. 23, no. 9. pp. 831–840, Sep-2001.

[39] J. Snellman *et al.*, "Acute destruction of the synaptic ribbon reveals a role for the ribbon in vesicle priming," *Nat. Neurosci.*, vol. 14, no. 9, pp. 1135–1143, Sep. 2011.

[40] B. W. Edmonds, F. D. Gregory, and F. E. Schweizer, "Evidence that fast exocytosis can be predominantly mediated by vesicles not docked at active zones in frog saccular hair cells," *Journal of Physiology*, vol. 560, no. 2. Wiley-Blackwell, pp. 439–450, 15-Oct-2004.

[41] P. A. Fuchs, "Time and intensity coding at the hair cell's ribbon synapse," *J. Physiol.*, vol. 566, no. 1, pp. 7–12, Jul. 2005.

[42] C. W. Graydon, S. Cho, G. L. Li, B. Kachar, and H. von Gersdorff, "Sharp Ca 2+ Nanodomains beneath the ribbon promote highly synchronous multivesicular release at hair cell synapses," *J. Neurosci.*, vol. 31, no. 46, pp. 16637–16650, Nov. 2011.

[43] H. Von Gersdorff, E. Vardi, G. Matthews, and P. Sterling, "Evidence that vesicles on the synaptic ribbon of retinal bipolar neurons can be rapidly released," *Neuron*, vol. 16, no. 6, pp. 1221–1227, 1996.

[44] T. Pangšrič *et al.*, "Hearing requires otoferlin-dependent efficient replenishment of synaptic vesicles in hair cells," *Nat. Neurosci.*, vol. 13, no. 7, pp. 869–876, Jul. 2010.

[45] D. Lenzi, J. Crum, M. H. Ellisman, and W. M. Roberts, "Depolarization redistributes synaptic membrane and creates a gradient of vesicles on the synaptic body at a ribbon

synapse," *Neuron*, vol. 36, no. 4, pp. 649–659, Nov. 2002.

[46] L. Siksou, F. Varoqueaux, O. Pascual, A. Triller, N. Brose, and S. Marty, "A common molecular basis for membrane docking and functional priming of synaptic vesicles," *Eur. J. Neurosci.*, vol. 30, no. 1, pp. 49–56, Jul. 2009.

[47] R. Fernández-Busnadiego *et al.*, "Cryo-electron tomography reveals a critical role of RIM1 α in synaptic vesicle tethering," *J. Cell Biol.*, vol. 201, no. 5, pp. 725–740, May 2013.

[48] A. Kantardzhieva, M. C. Liberman, and W. F. Sewell, "Quantitative analysis of ribbons, vesicles, and cisterns at the cat inner hair cell synapse: Correlations with spontaneous rate," *J. Comp. Neurol.*, vol. 521, no. 14, pp. 3260–3271, Oct. 2013.

[49] D. Mikaelian and R. J. Ruben, "Development of Hearing in the Normal Cba-J Mouse: Correlation of Physiological Observations with Behavioral Responses and with Cochlear Anatomy," *Acta Otolaryngol.*, vol. 59, no. 2–6, pp. 451–461, Jan. 1965.

[50] A. B. Wong *et al.*, "Developmental refinement of hair cell synapses tightens the coupling of Ca2+ influx to exocytosis," *EMBO J.*, vol. 33, no. 3, pp. 247–264, Feb. 2014.

[51] S. Michanski *et al.*, "Mapping developmental maturation of inner hair cell ribbon synapses in the apical mouse cochlea," *Proc. Natl. Acad. Sci.*, vol. 116, no. 13, pp. 6415–6424, Mar. 2019.

[52] R. T. Fremeau, "Vesicular Glutamate Transporters 1 and 2 Target to Functionally Distinct Synaptic Release Sites," *Science (80-.).*, vol. 304, no. 5678, pp. 1815–1819, Jun. 2004.

[53] S. Takamori, P. Malherbe, C. Broger, and R. Jahn, "Molecular cloning and functional characterization of human vesicular glutamate transporter 3," *EMBO Rep.*, vol. 3, no. 8, pp. 798–803, Aug. 2002.

[54] R. T. Fremeau *et al.*, "The identification of vesicular glutamate transporter 3 suggests novel modes of signaling by glutamate," *Proc. Natl. Acad. Sci. U. S. A.*, vol. 99, no. 22, pp. 14488–14493, Oct. 2002.

[55] N. Obholzer *et al.*, "Vesicular glutamate transporter 3 is required for synaptic transmission in zebrafish hair cells," *J. Neurosci.*, vol. 28, no. 9, pp. 2110–2118, Feb. 2008.

[56] J. Ruel *et al.*, "Impairment of SLC17A8 Encoding Vesicular Glutamate Transporter-3, VGLUT3, Underlies Nonsyndromic Deafness DFNA25 and Inner Hair Cell Dysfunction in Null Mice," *Am. J. Hum. Genet.*, vol. 83, no. 2, pp. 278–292, Aug. 2008.

[57] R. P. Seal *et al.*, "Sensorineural Deafness and Seizures in Mice Lacking Vesicular Glutamate Transporter 3," *Neuron*, vol. 57, no. 2, pp. 263–275, Jan. 2008.

[58] I. Roux *et al.*, "Otoferlin, Defective in a Human Deafness Form, Is Essential for Exocytosis at the Auditory Ribbon Synapse," *Cell*, vol. 127, no. 2, pp. 277–289, Oct. 2006.

[59] O. Akil *et al.*, "Restoration of Hearing in the VGLUT3 Knockout Mouse Using Virally Mediated Gene Therapy," *Neuron*, vol. 75, no. 2, pp. 283–293, Jul. 2012.

[60] R. H. Edwards, “The Neurotransmitter Cycle and Quantal Size,” *Neuron*, vol. 55, no. 6. pp. 835–858, 20-Sep-2007.

[61] S. Schenck, S. M. Wojcik, N. Brose, and S. Takamori, “A chloride conductance in VGLUT1 underlies maximal glutamate loading into synaptic vesicles,” *Nat. Neurosci.*, vol. 12, no. 2, pp. 156–162, Feb. 2009.

[62] G. Y. Goh *et al.*, “Presynaptic regulation of quantal size: K+/H+ exchange stimulates vesicular glutamate transport,” *Nat. Neurosci.*, vol. 14, no. 10, pp. 1285–1292, Oct. 2011.

[63] A. M. Smardon, M. Tarsio, and P. M. Kane, “The RAVE complex is essential for stable assembly of the yeast V-ATPase,” *J. Biol. Chem.*, vol. 277, no. 16, pp. 13831–13839, Apr. 2002.

[64] E. S. Trombetta, M. Ebersold, W. Garrett, M. Pypaert, and I. Mellman, “Activation of lysosomal function during dendritic cell maturation,” *Science (80-.).*, vol. 299, no. 5611, pp. 1400–1403, Feb. 2003.

[65] A. M. Smardon and P. M. Kane, “RAVE is essential for the efficient assembly of the C subunit with the vacuolar H+-ATPase,” *J. Biol. Chem.*, vol. 282, no. 36, pp. 26185–26194, Sep. 2007.

[66] D. J. Cipriano *et al.*, “Structure and regulation of the vacuolar ATPases,” *Biochim. Biophys. Acta - Bioenerg.*, vol. 1777, no. 7–8, pp. 599–604, Jul. 2008.

[67] Y. Feng and M. Forgac, “Inhibition of vacuolar H(+)-ATPase by disulfide bond formation between cysteine 254 and cysteine 532 in subunit A.,” *J. Biol. Chem.*, vol. 269, no. 18, pp. 13224–30, May 1994.

[68] L. Siksou *et al.*, “Three-dimensional architecture of presynaptic terminal cytomatrix,” *J. Neurosci.*, vol. 27, no. 26, pp. 6868–6877, Jun. 2007.

[69] R. Fernández-Busnadiego, B. Zuber, U. E. Maurer, M. Cyrklaff, W. Baumeister, and V. Lučić, “Quantitative analysis of the native presynaptic cytomatrix by cryoelectron tomography,” *J. Cell Biol.*, vol. 188, no. 1, pp. 145–156, Dec. 2010.

[70] C. Vogl *et al.*, “Unconventional molecular regulation of synaptic vesicle replenishment in cochlear inner hair cells,” *J. Cell Sci.*, vol. 128, no. 4, pp. 638–644, 2015.

[71] A. Betz *et al.*, “Functional interaction of the active zone proteins Munc13-1 and RIM1 in synaptic vesicle priming.,” *Neuron*, vol. 30, no. 1, pp. 183–96, Apr. 2001.

[72] T. Xu, T. Binz, H. Niemann, and E. Neher, “Multiple kinetic components of exocytosis distinguished by neurotoxin sensitivity,” *Nat. Neurosci.*, vol. 1, no. 3, pp. 192–200, 1998.

[73] T. Sakaba, “Distinct Kinetic Changes in Neurotransmitter Release After SNARE Protein Cleavage,” *Science (80-.).*, vol. 309, no. 5733, pp. 491–494, Jul. 2005.

[74] S. Safieddine and R. J. Wenthold, “SNARE complex at the ribbon synapses of cochlear hair cells: Analysis of synaptic vesicle- and synaptic membrane-associated proteins,” *Eur. J. Neurosci.*, vol. 11, no. 3, pp. 803–812, 1999.

[75] R. Nouvian *et al.*, “Exocytosis at the hair cell ribbon synapse apparently operates without neuronal SNARE proteins,” *Nat. Neurosci.*, vol. 14, no. 4, pp. 411–413, Apr. 2011.

[76] M. Beurg *et al.*, “Control of exocytosis by synaptotagmins and otoferlin in auditory hair

cells," *J. Neurosci.*, vol. 30, no. 40, pp. 13281–13290, Oct. 2010.

[77] E. Reisinger *et al.*, "Probing the functional equivalence of otoferlin and synaptotagmin 1 in exocytosis," *J. Neurosci.*, vol. 31, no. 13, pp. 4886–4895, Mar. 2011.

[78] N. Strenzke *et al.*, "Complexin-I is required for high-fidelity transmission at the endbulb of held auditory synapse," *J. Neurosci.*, vol. 29, no. 25, pp. 7991–8004, Jun. 2009.

[79] R. C. Uthaiah and A. J. Hudspeth, "Molecular anatomy of the hair cell's ribbon synapse," *J. Neurosci.*, vol. 30, no. 37, pp. 12387–12399, Sep. 2010.

[80] M. Beurg, S. Safieddine, I. Roux, Y. Bouleau, C. Petit, and D. Dulon, "Calcium- and otoferlin-dependent exocytosis by immature outer hair cells," *J. Neurosci.*, vol. 28, no. 8, pp. 1798–1803, Feb. 2008.

[81] D. Dulon, S. Safieddine, S. M. Jones, and C. Petit, "Otoferlin is critical for a highly sensitive and linear calcium-dependent exocytosis at vestibular hair cell ribbon synapses," *J. Neurosci.*, vol. 29, no. 34, pp. 10474–10487, Aug. 2009.

[82] S. Yasunaga *et al.*, "A mutation in OTOF, encoding otoferlin, a FER-1-like protein, causes DFNB9, a nonsyndromic form of deafness," *Nat. Genet.*, vol. 21, no. 4, pp. 363–369, Apr. 1999.

[83] R. Varga *et al.*, "OTOF mutations revealed by genetic analysis of hearing loss families including a potential temperature sensitive auditory neuropathy allele," *J. Med. Genet.*, vol. 43, no. 7, pp. 576–581, Jul. 2006.

[84] M. Rodríguez-Ballesteros *et al.*, "A multicenter study on the prevalence and spectrum of mutations in the otoferlin gene (OTOF) in subjects with nonsyndromic hearing impairment and auditory neuropathy," *Hum. Mutat.*, vol. 29, no. 6, pp. 823–831, Jun. 2008.

[85] C. Longo-Guess, L. H. Gagnon, D. E. Bergstrom, and K. R. Johnson, "A missense mutation in the conserved C2B domain of otoferlin causes deafness in a new mouse model of DFNB9," *Hear. Res.*, vol. 234, no. 1–2, pp. 21–28, Dec. 2007.

[86] M. Schwander *et al.*, "A forward genetics screen in mice identifies recessive deafness traits and reveals that pejvakin is essential for outer hair cell function," *J. Neurosci.*, vol. 27, no. 9, pp. 2163–2175, Feb. 2007.

[87] N. A. Ramakrishnan, M. J. Drescher, and D. G. Drescher, "Direct interaction of otoferlin with syntaxin 1A, SNAP-25, and the L-type voltage-gated calcium channel Ca v1.3," *J. Biol. Chem.*, vol. 284, no. 3, pp. 1364–1372, Jan. 2009.

[88] N. A. Ramakrishnan, M. J. Drescher, B. J. Morley, P. M. Kelley, and D. G. Drescher, "Calcium regulates molecular interactions of otoferlin with soluble NSF attachment protein receptor (SNARE) proteins required for hair cell exocytosis," *J. Biol. Chem.*, vol. 289, no. 13, pp. 8750–8766, Mar. 2014.

[89] C. P. Johnson and E. R. Chapman, "Otoferlin is a calcium sensor that directly regulates SNARE-mediated membrane fusion," *J. Cell Biol.*, vol. 191, no. 1, pp. 187–197, Oct. 2010.

[90] T. PangrŠič, E. Reisinger, and T. Moser, "Otoferlin: A multi-C 2 domain protein essential

for hearing," *Trends in Neurosciences*, vol. 35, no. 11. pp. 671–680, Nov-2012.

[91] R. Jahn, T. Lang, and T. C. Südhof, "Membrane Fusion," *Cell*, vol. 112, no. 4, pp. 519–533, Feb. 2003.

[92] L. J. Robinson and T. F. Martin, "Docking and fusion in neurosecretion," *Curr. Opin. Cell Biol.*, vol. 10, no. 4, pp. 483–492, Aug. 1998.

[93] D. Fasshauer, R. B. Sutton, A. T. Brunger, and R. Jahn, "Conserved structural features of the synaptic fusion complex: SNARE proteins reclassified as Q- and R-SNAREs," *Proc. Natl. Acad. Sci. U. S. A.*, vol. 95, no. 26, pp. 15781–15786, Dec. 1998.

[94] T. C. Südhof, "THE SYNAPTIC VESICLE CYCLE," *Annu. Rev. Neurosci.*, vol. 27, no. 1, pp. 509–547, Jul. 2004.

[95] I. Augustin, C. Rosenmund, T. C. Südhof, and N. Brose, "Munc13-1 is essential for fusion competence of glutamatergic synaptic vesicles," *Nature*, vol. 400, no. 6743, pp. 457–461, Jul. 1999.

[96] T. D. Parsons and P. Sterling, "Synaptic ribbon: Conveyor belt or safety belt?," *Neuron*, vol. 37, no. 3. Cell Press, pp. 379–382, 06-Feb-2003.

[97] E. Glowatzki and P. A. Fuchs, "Transmitter release at the hair cell ribbon synapse," *Nat. Neurosci.*, vol. 5, no. 2, pp. 147–154, 2002.

[98] A. Neef, D. Khimich, P. Pirih, D. Riedel, F. Wolf, and T. Moser, "Probing the mechanism of exocytosis at the hair cell ribbon synapse," *J. Neurosci.*, vol. 27, no. 47, pp. 12933–12944, Nov. 2007.

[99] N. M. Chapochnikov *et al.*, "Uniquantal release through a dynamic fusion pore is a candidate mechanism of hair cell exocytosis," *Neuron*, vol. 83, no. 6, pp. 1389–1403, 2014.

[100] C. W. Graydon, J. Zhang, N. W. Oesch, A. A. Sousa, R. D. Leapman, and J. S. Diamond, "Passive diffusion as a mechanism underlying ribbon synapse vesicle release and resupply," *J. Neurosci.*, vol. 34, no. 27, pp. 8948–8962, 2014.

[101] D. N. Furness and K. P. Lehre, "Immunocytochemical localization of a high-affinity glutamate-aspartate transporter, GLAST, in the rat and guinea-pig cochlea," *Eur. J. Neurosci.*, vol. 9, no. 9, pp. 1961–1969, Sep. 1997.

[102] D. N. Furness and D. M. Lawton, "Comparative Distribution of Glutamate Transporters and Receptors in Relation to Afferent Innervation Density in the Mammalian Cochlea," *J. Neurosci.*, vol. 23, no. 36, pp. 11296–11304, Dec. 2003.

[103] G. Rebillard *et al.*, "Glutamate transporters in the guinea-pig cochlea: Partial mRNA sequences, cellular expression and functional implications," *Eur. J. Neurosci.*, vol. 17, no. 1, pp. 83–92, 2003.

[104] F. Nagano *et al.*, "Rabconnectin-3, a novel protein that binds both GDP/GTP exchange protein and GTPase-activating protein for Rab3 small G protein family," *J. Biol. Chem.*, vol. 277, no. 12, pp. 9629–9632, Mar. 2002.

[105] H. Kawabe *et al.*, "A novel rabconnectin-3-binding protein that directly binds a GDP/GTP exchange protein for Rab3A small G protein implicated in Ca2+-dependent exocytosis of

neurotransmitter," *Genes to Cells*, vol. 8, no. 6, pp. 537–546, Jun. 2003.

[106] A. M. Tuttle, T. L. Hoffman, and T. F. Schilling, "Rabconnectin-3a Regulates Vesicle Endocytosis and Canonical Wnt Signaling in Zebrafish Neural Crest Migration," *PLoS Biol.*, vol. 12, no. 5, p. e1001852, May 2014.

[107] "DMXL2 - DmX-like protein 2 - Homo sapiens (Human) - DMXL2 gene & protein." [Online]. Available: https://www.uniprot.org/uniprot/Q8TDJ6. [Accessed: 20-May-2020].

[108] K. Wan Li, N. Chen, P. Klemmer, F. Koopmans, R. Karupothula, and A. B. Smit, "Identifying true protein complex constituents in interaction proteomics: The example of the DMXL2 protein complex," *Proteomics*, vol. 12, no. 15–16, pp. 2428–2432, Aug. 2012.

[109] C. U. Stirnimann, E. Petsalaki, R. B. Russell, and C. W. Müller, "WD40 proteins propel cellular networks," *Trends Biochem. Sci.*, vol. 35, no. 10, pp. 565–574, Oct. 2010.

[110] Y. Yan, N. Denef, and T. Schüpbach, "The Vacuolar Proton Pump, V-ATPase, Is Required for Notch Signaling and Endosomal Trafficking in Drosophila," *Dev. Cell*, vol. 17, no. 3, pp. 387–402, Sep. 2009.

[111] N. Sethi, Y. Yan, D. Quek, T. Schupbach, and Y. Kang, "Rabconnectin-3 is a functional regulator of mammalian notch signaling," *J. Biol. Chem.*, vol. 285, no. 45, pp. 34757–34764, Nov. 2010.

[112] Z. Einhorn, J. G. Trapani, Q. Liu, and T. Nicolson, "Rabconnectin3α promotes stable activity of the H + pump on synaptic vesicles in hair cells," *J. Neurosci.*, vol. 32, no. 32, pp. 11144–11156, Aug. 2012.

[113] D. Y. Chen *et al.*, "A dominant variant in DMXL2 is linked to nonsyndromic hearing loss," *Genet. Med.*, vol. 19, no. 5, pp. 553–558, May 2017.

[114] Y. Yan, N. Denef, and T. Schüpbach, "The Vacuolar Proton Pump, V-ATPase, Is Required for Notch Signaling and Endosomal Trafficking in Drosophila," *Dev. Cell*, vol. 17, no. 3, pp. 387–402, Sep. 2009.

[115] J. P. Sumner, J. A. T. Dow, F. G. P. Earley, U. Klein, D. Jager, and H. Wieczorek, "Regulation of plasma membrane V-ATPase activity by dissociation of peripheral subunits," *J. Biol. Chem.*, vol. 270, no. 10, pp. 5649–5653, Mar. 1995.

[116] M. A. Gandini, I. A. Souza, J. Fan, K. Li, D. Wang, and G. W. Zamponi, "Interactions of Rabconnectin-3 with Cav2 calcium channels," *Mol. Brain*, vol. 12, no. 1, p. 62, Dec. 2019.

[117] M. Tanaka *et al.*, "Role of Rab3 GDP/GTP exchange protein in synaptic vesicle trafficking at the mouse neuromuscular junction," *Mol. Biol. Cell*, vol. 12, no. 5, pp. 1421–1430, May 2001.

[118] S. Niwa, Y. Tanaka, and N. Hirokawa, "KIF1Bβ- and KIF1A-mediated axonal transport of presynaptic regulator Rab3 occurs in a GTP-dependent manner through DENN/MADD," *Nat. Cell Biol.*, vol. 10, no. 11, pp. 1269–1279, Nov. 2008.

[119] E. R. Graf, R. W. Daniels, R. W. Burgess, T. L. Schwarz, and A. DiAntonio, "Rab3 Dynamically Controls Protein Composition at Active Zones," *Neuron*, vol. 64, no. 5, pp.

663–677, Dec. 2009.

[120] B. Tata *et al.*, “Haploinsufficiency of Dmxl2, Encoding a Synaptic Protein, Causes Infertility Associated with a Loss of GnRH Neurons in Mouse,” *PLoS Biol.*, vol. 12, no. 9, 2014.

[121] C. Gobé *et al.*, “Dual role of DMXL2 in olfactory information transmission and the first wave of spermatogenesis,” *PLOS Genet.*, vol. 15, no. 2, p. e1007909, Feb. 2019.

[122] M. Kannan *et al.*, “WD40-repeat 47, a microtubule-associated protein, is essential for brain development and autophagy,” *Proc. Natl. Acad. Sci. U. S. A.*, vol. 114, no. 44, pp. E9308–E9317, Oct. 2017.

[123] G. Costain *et al.*, “Rare copy number variations affecting the synaptic gene DMXL2 in neurodevelopmental disorders,” *J. Neurodev. Disord.*, vol. 11, no. 1, p. 3, Feb. 2019.

[124] “OMIM Entry - # 616113 - POLYENDOCRINE-POLYNEUROPATHY SYNDROME; PEPNS.” [Online]. Available: https://www.omim.org/entry/616113. [Accessed: 30-May-2020].

[125] B. K. Tata, C. Harbulot, Z. Csaba, S. Peineau, S. Jacquier, and N. De Roux, “Rabconnectin-3α is required for the morphological maturation of GnRH neurons and kisspeptin responsiveness,” *Sci. Rep.*, vol. 7, no. 1, pp. 1–12, Feb. 2017.

[126] A. Esposito *et al.*, “Biallelic DMXL2 mutations impair autophagy and cause Ohtahara syndrome with progressive course,” *Brain*, vol. 142, no. 12, pp. 3876–3891, Dec. 2019.

[127] T. Nicolson, “The Genetics of Hearing and Balance in Zebrafish,” *Annu. Rev. Genet.*, vol. 39, no. 1, pp. 9–22, Dec. 2005.

[128] S. Safieddine, A. El-Amraoui, and C. Petit, “The Auditory Hair Cell Ribbon Synapse: From Assembly to Function,” *Annu. Rev. Neurosci.*, vol. 35, no. 1, pp. 509–528, Jul. 2012.

[129] B. Pan and J. R. Holt, “The molecules that mediate sensory transduction in the mammalian inner ear,” *Curr. Opin. Neurobiol.*, vol. 34, pp. 165–171, Oct. 2015.

[130] K. S. Kindt and L. Sheets, “Transmission Disrupted: Modeling Auditory Synaptopathy in Zebrafish,” *Front. Cell Dev. Biol.*, vol. 6, Sep. 2018.

[131] H. Kim, M. Kim, S.-K. Im, and S. Fang, “Mouse Cre-LoxP system: general principles to determine tissue-specific roles of target genes,” *Lab. Anim. Res.*, vol. 34, no. 4, p. 147, 2018.

[132] Z. Peng, G.-P. Wang, R. Zeng, J.-Y. Guo, C.-F. Chen, and S.-S. Gong, “Temporospatial expression and cellular localization of VGLUT3 in the rat cochlea,” *Brain Res.*, vol. 1537, no. 5, pp. 100–110, Nov. 2013.

[133] A. G. M. Leenders, F. H. Lopes da Silva, W. E. J. M. Ghijsen, and M. Verhage, “Rab3A is involved in transport of synaptic vesicles to the active zone in mouse brain nerve terminals,” *Mol. Biol. Cell*, vol. 12, no. 10, pp. 3095–3102, 2001.

[134] Y. Lee, H. R. Kim, and S. C. Ahn, “Vesicular glutamate transporter 3 is strongly upregulated in cochlear inner hair cells and spiral ganglion cells of developing circling mice,” *Neurosci. Lett.*, vol. 584, pp. 320–324, Jan. 2015.

[135] P. T. Ranum *et al.*, “Insights into the Biology of Hearing and Deafness Revealed by Single-Cell RNA Sequencing,” *Cell Rep.*, vol. 26, no. 11, pp. 3160-3171.e3, Mar. 2019.

[136] A. Amsterdam, R. M. Nissen, Z. Sun, E. C. Swindell, S. Farrington, and N. Hopkins, “Identification of 315 genes essential for early zebrafish development,” *Proc. Natl. Acad. Sci.*, vol. 101, no. 35, pp. 12792–12797, Aug. 2004.

[137] S.-Y. Lin, M. A. Vollrath, S. Mangosing, J. Shen, E. Cardenas, and D. P. Corey, “The zebrafish pinball wizard gene encodes WRB, a tail-anchored-protein receptor essential for inner-ear hair cells and retinal photoreceptors,” *J. Physiol.*, vol. 594, no. 4, pp. 895–914, Feb. 2016.

[138] C. Vogl *et al.*, “Tryptophan-rich basic protein (WRB) mediates insertion of the tail-anchored protein otoferlin and is required for hair cell exocytosis and hearing,” *EMBO J.*, vol. 35, no. 23, pp. 2536–2552, Dec. 2016.